ELECTROLYTIC DESTRUCTION OF CYANIDE ON BARE AND MnO_2 COATED 304 STAINLESS STEEL ELECTRODES

By

Jacob Schmidt

A thesis submitted in partial fulfillment
of the requirements for the degree of
Master of Applied Science (M.A.Sc.)
in Natural Resource Engineering

The Faculty of Graduate Studies
Laurentian University
Sudbury, Ontario, Canada

THESIS DEFENCE COMMITTEE/COMITÉ DE SOUTENANCE DE THÈSE
Laurentian Université/Université Laurentienne
Office of Graduate Studies/Bureau des études supérieures

Title of Thesis
Titre de la thèse: Electrolytic destruction of cyanide on bare and MnO2 coated 304 stainless steel electrodes

Name of Candidate
Nom du candidat: Schmidt, Jacob

Degree
Diplôme: Master of Science

Department/Program
Département/Programme: Engineering

Date of Defence
Date de la soutenance: Septembre 15, 2021

APPROVED/APPROUVÉ

Thesis Examiners/Examinateurs de thèse:

Dr. Eduard Guerra
(Supervisor/Directeur(trice) de thèse)

Dr. Jeffrey Shepherd
(Co-supervisor/Co-directeur(trice) de thèse)

Dr. Corey Laamanen
(Committee member/Membre du comité)

Dr. Ahmad Ghahreman
(External Examiner/Examinateur externe)

Approved for the Office of Graduate Studies
Approuvé pour le Bureau des études supérieures
Tammy Eger, PhD
Vice-President Research (Office of Graduate Studies)
Vice-rectrice à la recherche (Bureau des études supérieures)
Laurentian University / Université Laurentienne

ACCESSIBILITY CLAUSE AND PERMISSION TO USE

Contents

ABSTRACT

MnO_2 coated lead and ANSI-304 stainless steel anodes were evaluated for use in electrolytic cyanide waste effluent treatment. Cyclic voltametry experiments revealed that MnO_2 on lead was too resistive to be a feasible substrate. Cyclic voltammetry on bare and MnO_2 coated steel shows evidence of cyanide destruction just prior to the onset of massive oxygen evolution, suggesting a reaction mechanism in which cyanide is oxidized via reaction with hydroxide radical species on the electrode surface. Galvanostatic experiments showed little difference in cyanide oxidation performance behaviour between bare steel and the MnO_2 coating. However, copper ion were found to catalyse cyanide oxidation for bare steel, but had no observed effect for MnO_2 coated steel. A cost analysis was done comparing electrolytic cyanide destruction using bare steel anodes to the INCO SO_2/Air process. Electrolytic cyanide oxidation was concluded to have significantly lower operating costs, but is infeasible due to prohibitive capital costs.

1 INTRODUCTION

Although cyanide is extremely toxic, cyanidization was used for 90% of primary gold extraction as of 2002, with physical separation being used for the remaining 10% [1]. The half-reaction for cyanidization of gold appears as Equation 1-1 [2]. Cyanide depresses the standard electrode potential for reduction of gold ions, allowing it to be oxidized by even mild oxidizing agents. The effect is most noticeable at high pH (where the bulk of cyanide in solution exists as CN^- ions as opposed to $HCN_{(aq)}$); see Figure 1-1 which shows the reduction potential of $\mathrm{Au(CN)_2^-} \rightarrow \mathrm{Au(s)}$ stabilize at a relatively low value above pH 9. [3] For this reason, in conjunction with the volatility of hydrocyanic acid, cyanide leaching of gold ore is typically done under caustic conditions.

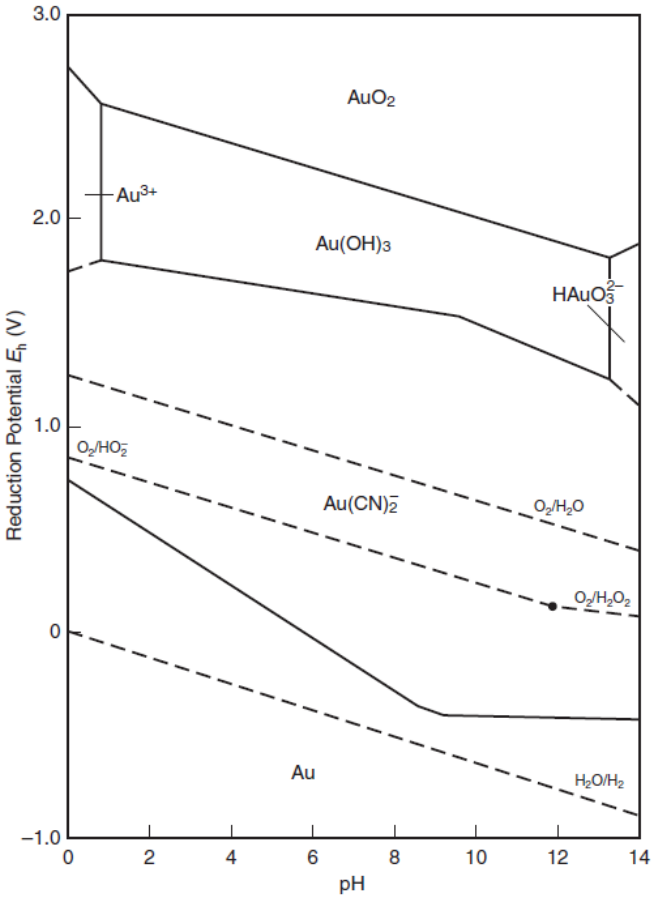

Figure 0-1: Pourbaix diagram for Au-H_2O-CN^- C_{Au}= 10^{-4}M, C_{CN^-} = 10^{-3}, pO_2/H_2 = 1atm. Modified from [3].

$$E^\circ = -0.67V \qquad Au(CN)_2^- + e^- \rightarrow Au + 2CN^- \qquad 1\text{-}1$$

$$E^\circ = 1.59\mathrm{V} \qquad Au^{3+} + 3e^- \rightarrow Au \qquad 1\text{-}2$$

The waste tailings generated from cyanide leaching were historically discharged into shallow tailings ponds where cyanide concentration diminished over time by a combination of natural volatilization and oxidation by reaction with dissolved oxygen from the air, catalyzed by ultraviolet light from the sun. Major spills from these ponds have occurred in several instances, including an incident in South Africa in 1994 leaving 17 dead, and an instance in New Zealand in 1995 contaminating the water table [4]. As a result of these risks, Canadian regulations require that mill effluent contain at most an average of 1 ppm of cyanide per month, and never exceed 2 ppm cyanide [5].

1.1 CHEMICAL CYANIDE DESTRUCTION

Waste cyanide bearing effluent is typically treated with chemical reagents. The INCO SO_2/Air process is by far the most widely used for treatment of industrial gold cyanide waste streams. In laboratory environments, potassium permanganate is often used to treat small volumes of waste cyanide solutions.

1.1.1 INCO SO_2/Air Process

The INCO SO_2/Air process introduces sulphite into solution, either directly through dissolution of sulphite salts or by introducing sulphur dioxide liquid which reacts to form sulphite and acid. [6]

$$SO_2 + H_2O \rightarrow SO_3^{2-} + 2H^+ \qquad \textit{1-3}$$

Oxygen is then introduced to solution through forced air dissolution. Sulphite and oxygen react with cyanide to form cyanate and sulphate.

$$CN^- + SO_3^{2-} + O_2 \rightarrow SO_4^{2-} + OCN^- \qquad 1\text{-}4$$

The primary cost for this method is the SO_2 source. In practice, SO_2 is added to an excess between 22% and 103%. [7] This reaction is carried out in mildly basic conditions. Typically, lime is added in conjunction with SO_2 to keep the pH at an appropriate level.

A small amount of copper ions in solution is necessary to achieve acceptable rates of cyanide oxidation [8]. Copper is typically added to solution by dissolution of copper sulfate. It is believed that the copper(II) ions react with cyanide to form a cupric cyanide complex, $[Cu_2(CN)_6]^{2-}$, that subsequently decomposes into a copper(I) cyanide complex, $[Cu(CN)_3]^-$, and cyanogen, $(CN)_2$ [9].

$$[Cu_2(CN)_6]^{2-} \rightarrow 2[Cu(CN)_2]^- + (CN)_2 \qquad 1\text{-}5$$

The cyanogen then reacts with hydroxide ions to from cyanide and cyanate according to the following reaction [8]:

$$(CN)_2 + OH^- \rightarrow CN^- + OCN^- + H^+ \qquad 1\text{-}6$$

Further cyanide destruction relies on the catalytic effect of copper (I) cyanide complexes, as illustrated in Equations 1-7 and 1-8. The reactions described in Equations 1-7 and 1-8 are extremely favourable, with equilibrium constants on the order of 10^8 and 10^5 respectively. This allows copper to act as a scavenger, pulling cyanide off other metals to form the copper(I) complexes that catalyze cyanide oxidation. This allows for the destruction of cyanide that is complexed with Ni, Zn, Cd, Hg, and Ag, which is called weak acid dissociable (WAD) cyanide.

$$Cu^{+} + 2CN^{-} \leftrightarrow [Cu(CN)_2]^{-} \quad 1\text{-}7$$

$$[Cu(CN)_2]^{-} + CN^{-} \leftrightarrow [Cu(CN)_3]^{2-} \quad 1\text{-}8$$

$$[Cu(CN)_3]^{2-} + SO_3^{2-} + O_2 \rightarrow [Cu(CN)_2]^{-} + SO_4^{2-} + OCN^{-} \quad 1\text{-}9$$

Without the addition of copper, the SO_2/Air process is infeasible. Notably, in the presence of cyanide, the natural oxidation of sulphite to sulphate is impeded (Figure 1-2). It is suggested

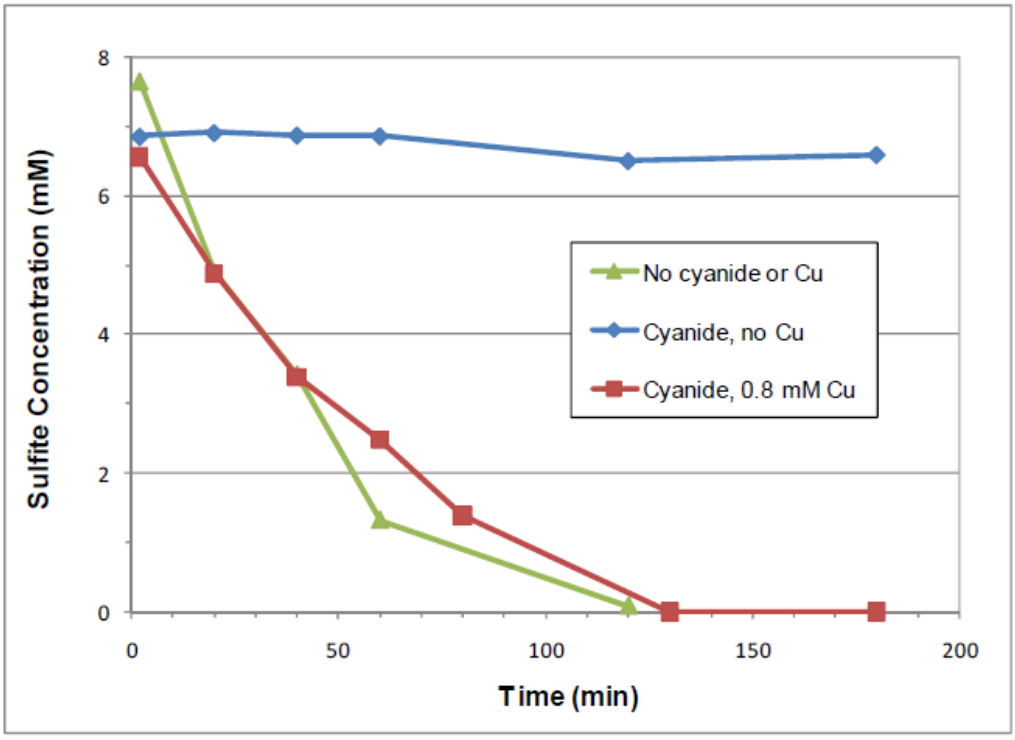

Figure 1-2: sulphite concentrations of 8mM Na_2SO_3 over time in an air sparged solution in the presence of cyanide and copper ions. Modified from [9].

that cyanide acts as a free radical scavenger [10], effectively stabilizing both itself and sulphite over time. In the presence of copper, however, sulphite is oxidized as normal, and cyanide along with it.

1.1.2 Potassium Permanganate

Permanganate ions are particularly fast and effective at oxidizing cyanide, and are effective at a wider range of pH (see Figure 1-3). Sodium hypochlorite performs to similar

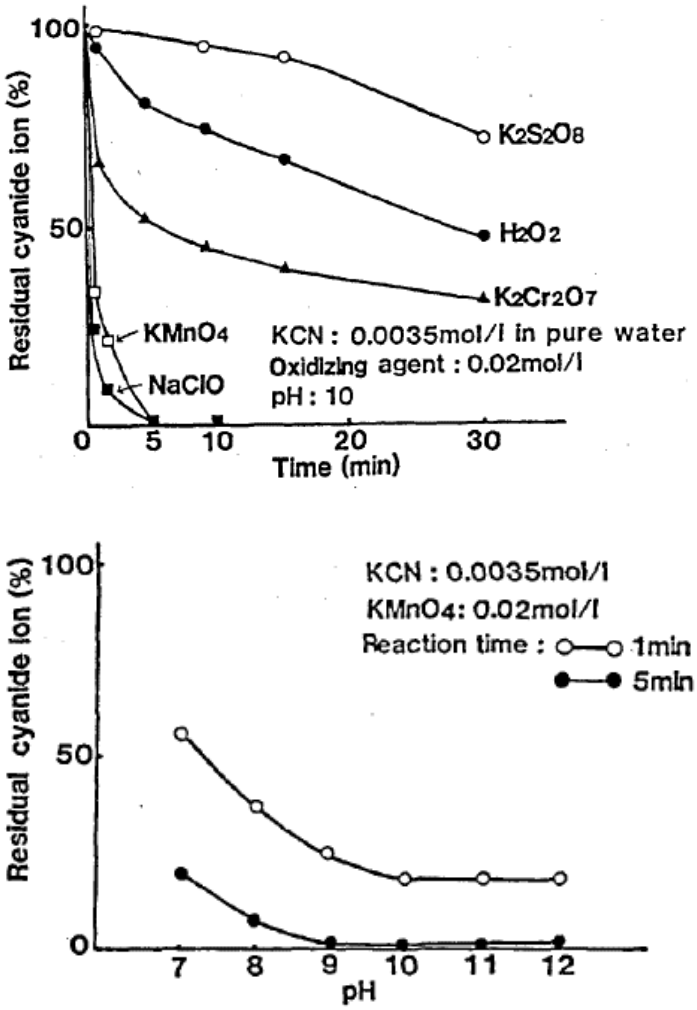

Figure 1-3: Top: residual cyanide concentration over time with exposure to strong chemical oxidant; bottom: residual cyanide concentration by pH with exposure to $KMnO_4$ after 1 and 5 minutes. Modified from [15].

effectiveness but produces toxic cyanogen chloride as a byproduct. Permanganate produces only manganese dioxide as a byproduct, which precipitates from solution immediately. As result, potassium permanganate is frequently used for lab scale disposal of cyanide waste.

$$2\mathrm{MnO_4^-} + 3\mathrm{CN^-} + \mathrm{H_2O} \rightarrow 2\mathrm{MnO_{2(s)}} + 3\mathrm{CNO^-} + 2\mathrm{OH^-} \quad \textit{1-10}$$

$$2\mathrm{MnO_4^-} + 2\mathrm{CNO^-} + 2\mathrm{H_2O} \rightarrow 2\mathrm{MnO_{2(s)}} + 2\mathrm{CO_2} + 4\mathrm{OH^-} \quad \textit{1-11}$$

Permanganate is not used industrially, however, largely due to the cost of reagents. A related concern is the tendency for permanganate to oxidize cyanate to carbon dioxide and nitrogen gas. [6] The wasted reagent on side reactions makes the already costly method even less cost effective.

1.2 ELECTROCHEMICAL CYANIDE DESTRUCTION

As opposed to the chemical methods for cyanide destruction, that involve homogeneous reactions in solution, electrolytic cyanide destruction involves heterogeneous half-cell reactions that occur at electrode surfaces. The overall half reaction for cyanide oxidation to cyanate is described below.

$$CN^- + H_2O \rightarrow OCN^- + 2H^+ + 2e^- \quad \textit{1-12}$$

The mechanism for cyanide oxidation at a copper electrode surface has been proposed by Wels & Johnson and Hine et al. [11] [12] to proceed via reaction with copper(III) hydroxide, $Cu(OH)_3$, sites at potentials where oxygen evolution occurs. Kelsall et al. [13] proposed a similar mechanism for cyanide oxidation at nickel anodes, where cyanide was oxidized at nickel (III) hydroxide, $Ni(OH)_3$, sites. In this regard, Comninellis [14] suggests a general multi-step model for oxidation of organics concomitant with oxygen evolution.

$$MO_x + H_2O \overset{k_1}{\rightarrow} MO_x(OH) + H^+ + e^- \quad \textit{1-13}$$

$$MO_x(OH) \overset{k_2}{\rightarrow} MO_{x+1} + H^+ + e^- \quad \textit{1-14}$$

$$MO_x(OH) \overset{k_o}{\rightarrow} \frac{1}{2}O_2 + H^+ + e^- + MO_x \quad \textit{1-15}$$

$$MO_{x+1} \overset{k_d}{\rightarrow} MO_x + \frac{1}{2}O_2 \quad \textit{1-16}$$

Equation 1-13 shows the physisorption of oxygen radicals, while Equation 1-14 shows the subsequent chemisorption of oxygen into the oxide layer of the electrode. Oxygen evolution follows as per Equations 1-15 and 1-16. Comninellis suggests that oxidation of organics occurs in parallel to these reactions. Where R is an arbitrary organic molecule:

$$MO_x(OH) + R \overset{k_c}{\rightarrow} CO_2 + ZH^+ + Ze^- + MO_x \quad \textit{1-17}$$

$$MO_{x+1} + R \overset{k_g}{\rightarrow} RO + MO_x \quad \textit{1-18}$$

Equation 1-17 shows total oxidation of the organic, while Equation 1-18 shows partial oxidation. Since cyanide is known to oxidize in two steps (from cyanide to cyanate, and from cyanate to carbon dioxide), we expect the mechanism to follow Equations 1-13 — 1-14—1-18.

1.2.1 Electrolytic copper catalysis of cyanide oxidation

The copper(I) cyanide complex, formed via Equation 1-8, has been suggested to catalyze electrolytic cyanide oxidation in weakly alkaline conditions, following a multi-step oxidation process producing a copper(I) cyanide complex and cyanogen [8]. Cyanogen is then transported back into the bulk where it reacts with hydroxide to form cyanide and cyanate as previously indicated [8]:

$$2[Cu(CN)_3]^{2-} \rightarrow 2[Cu(CN)_2]^- + (CN)_2 + 2e^- \quad \textit{1-19}$$

$$2[Cu(CN)_2]^- + 2CN^- \rightarrow 2[Cu(CN)_3]^{2-} \quad \textit{1-20}$$

However, in strongly alkaline conditions, the formation of the intermediate cyanogen is lost, and the reaction instead follows Equation 1-21. [15]

$$\mathrm{Cu(CN)_n^{(n-1)-} + 2nOH^- \rightarrow\ Cu^+ + nCNO^- + nH_2O + 2ne^-} \qquad \textit{1-21}$$

1.2.2 Kinetics of Electrolytic cyanide destruction

It has been shown that during electrolysis of dilute cyanide solutions, at sufficient current density, cyanide is oxidized under a pseudo 1st order regime. [15] [16]

$$\frac{\mathrm{d}C_{\mathrm{CN^-}}(t)}{\mathrm{d}t} = k_{CN^-}C_{\mathrm{CN^-}}(t) \qquad \textit{1-22}$$

$$C_{\mathrm{CN^-}}(t) = C_{\mathrm{CN^-}}(0)\mathrm{e}^{k_{\mathrm{CN^-}}\,t} \qquad \textit{1-23}$$

In this regard, it is likely that cyanide oxidation is mass transfer limited and that the value of the rate constant is affected by the nature of oxygen gas bubble evolution on the electrode surface and the concomitant micro-convective transport of cyanide to the electrode surface. Table 1-1 and Table 1-2 provides a summary of the rate constants and current efficiencies for cyanide oxidation, determined by Lanza and Bertazzoli [16] for several different anode materials under strongly alkaline conditions (pH>12).

*Table 1-1: Comparison of average k_{CN^-} values by anode material. *Multiple values for Graphite Raschig rings were reported.*

$k_{CN^-} \times 10^{-4}$ *(m/s)*	*Anode material*
0.47	$\mathrm{SnO_2 - Sb_2O_5}$
0.7	Stainless steel 316

0.1 & 0.17	Graphite Raschig rings*
0.2	Reticulated vitreous carbon (RVC)
0.2	$\mathrm{RVC - PbO_2}$
2.2	DSA ($\mathrm{Ti/70TiO_2/30RuO_2}$ w/w)

Hine et al. studied the current efficiency of cyanide oxidation on lead coated DSA anodes [12]. As illustrated in Figure 1-4, they found that lead performed significantly better than materials like platinum and 304 stainless steel. However, these current efficiencies require very high concentrations of cyanide to be realized and experiments were performed using copper free electrolytes. The minimum concentration reported for 100% current efficiency on lead coated DSAs (0.25M) is several orders of magnitude greater than the concentration of cyanide found in waste effluents in industry.

Table 1-2: Comparison of current efficiencies across several anode materials.

Current Efficiency	*Anode material*	*Concentration Range (M)*
100%	Electrodeposited $\mathrm{PbO_2}$	0.25-1.0
44%	Pt	0.79-1.0
34%	304 Stainless steel	0.84-1.0
90%	Pb	0.46-0.73
80%	Graphite	0.23-0.46

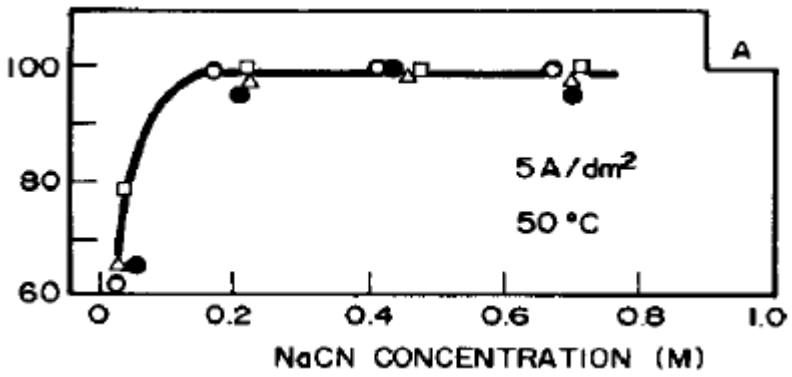

Figure 1-4: Current efficiency of cyanide oxidation on PbO_2 coated DSA anodes by cyanide concentration. Modified from [12].

Because of their excellent current efficiency for cyanide destruction relative to other substrates, lead electrodes were selected for further study.

1.3 MANGANESE DIOXIDE COATINGS

Manganese dioxide surfaces have been shown to be electroactive. In particular, MnO_2 surfaces have been demonstrated to be effective for oxygen reduction and evolution for use in lithium oxygen batteries [17] and zinc electrowinning [18]. If, as Comninellis [14] suggests, cyanide is oxidized concomitantly with oxygen evolution, it is plausible the catalytic effect MnO_2 has on oxygen evolution may also apply to cyanide oxidation. Additionally, moderate polarization of the MnO_2 anode may be particularly beneficial for cyanide destruction. Figure 1-5 shows a Pourbaix diagram of the Mn-H_2O system built in FactSage. By polarizing the MnO_2 anode to potential near the MnO_2/MnO_4^- boundary, oxygen evolution (likely necessary to oxidize cyanide) is thermodynamically favorable without dissolution of the MnO_2 layer to MnO_4^-.

The potential of using a permanent MnO_2 layer to catalyze cyanide destruction, as opposed to continuous addition of potassium permanganate was deemed to merit further

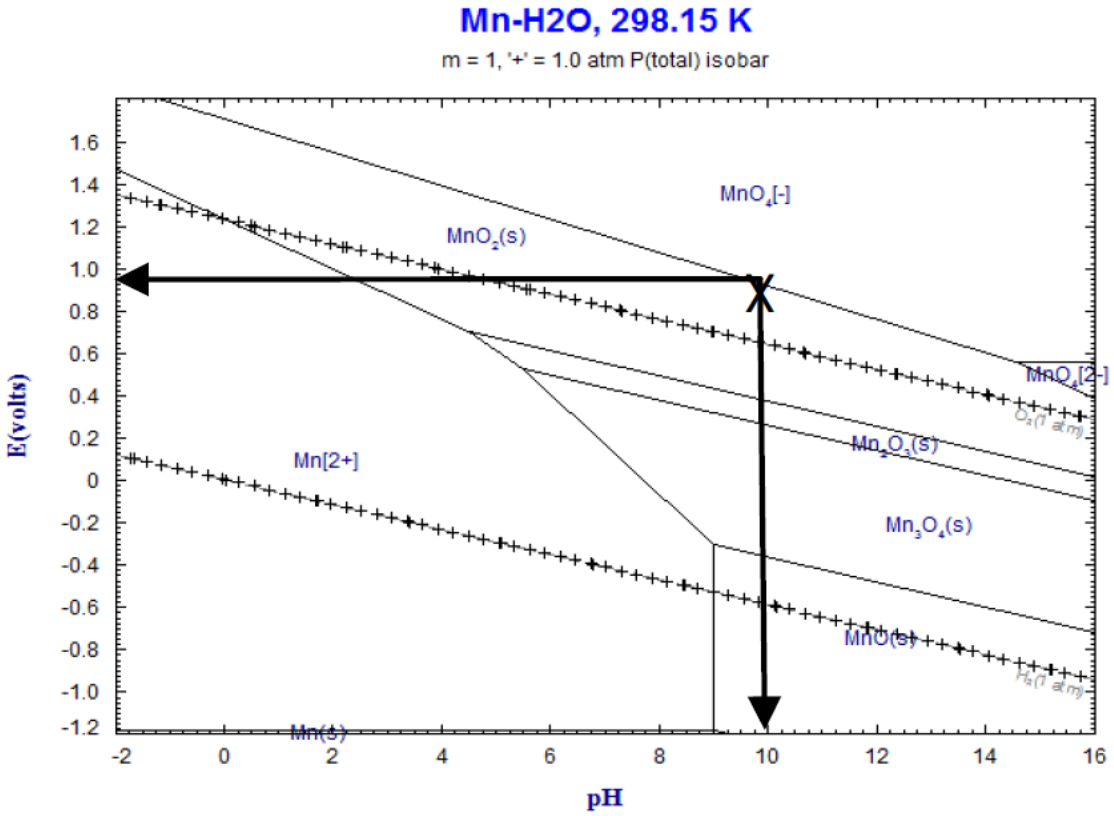

Figure 1-5: Pourbaix diagram of the Mn-H_2O system.

study. As a result, it was decided to explore different methods for creating a MnO_2 layer on lead electrodes. Two methods for producing these layers were explored: the industrial method for coating MnO_2 on lead electrodes for zinc electrowinning as well direct electrodeposition of MnO_2 from manganese solutions that had been reportedly employed for coating various electrode substrates in lithium batteries.

1.3.1 MnO_2 Coating of Pb electrodes for Zinc Electrowinning

Manganese dioxide coated Pb electrodes are used in zinc electrowinning to catalyze oxygen evolution and protect the underlying Pb substrate from corrosion. The MnO_2 is deposited by oxidizing the lead surface in the presence of sulfuric acid and an elevated temperature (~70°C) according to the following reaction:

$$4MnO_4^- + 4H^+ + 3Pb \rightarrow 3PbO_2 + 4MnO_2 + 2H_2O \quad \textit{1-24}$$

The catalytic MnO_2 layer then lowers the voltage requirement of the oxygen evolution half reaction, which lowers the power requirement (and ultimately lowers the cost) of zinc electrowinning.

1.3.2 MnO_2 Coating of Electrodes in Lithium-Oxygen batteries

Lithium-Oxygen batteries, on discharge, work through the formation of Lithium ions at the anode and either the formation of oxygen or the formation of lithium oxide at the cathode in aqueous and non-aqueous systems, respectively. [17]

$$Li \leftrightarrow Li^+ + e^- \quad \textit{1-25}$$

Alkaline $$O_2 + 2H_2O + 4e^- \leftrightarrow 4OH^- \quad \textit{1-26}$$

Acidic $$2H^+ + O_2 + 4e^- \rightarrow 2OH^- \quad \textit{1-27}$$

Non-aqueous $$2Li^+ + 2e^- + O_2 \leftrightarrow Li_2O_2 \quad \textit{1-28}$$

Several methods have been developed for creating MnO_2 layers on various substrate electrodes to catalyze the reactions in such batteries. Wei et al. [17] employ galvanostatic deposition from manganese acetate in the presence of sodium sulphate. Jacob & Zhitomirsky [19] employ a similar method using galvanostatic reduction from a solution of potassium permanganate.

$$MnO_4^- + 2H_2O + 3e^- \rightarrow MnO_2 + 4OH^- \quad \textit{1-29}$$

1.4 THESIS GOALS

This work aims to study the effectiveness of MnO_2 coated anodes for use in electrolytic oxidation of cyanide waste, beginning with the adoption of Pb-MnO_2 anodes as used in zinc

electrowinning. This is expected to be effective as MnO_2 is catalytic for oxygen evolution, and cyanide oxidation depends on the precursor steps to oxygen evolution. Additionally, it is hoped that polarization of the MnO_2 layer will allow it to act in a similar manner as MnO_4^-. The role of copper as an additional catalyst will be studied. The effectiveness of the catalyst layer will be explored galvanostatically and, if possible, the rate limiting conditions will be explored. Once the effectiveness is measured, the cost efficiency of an electrolysis plant will be explored.

2 LEAD AS A SUBSTRATE

MnO_2 coated lead electrodes were characterized using cyclic voltammetry to determine their suitability for cyanide oxidation.

2.1 MNO2 COATING OF LEAD ELECTRODES

Lead electrodes, which were constructed for use zinc mini electrowinning cells [20] were coated with an MnO_2 layer using an established process [18]. The electrodes themselves were comprised of a section of industrial Pb based anode, embedded in epoxy, with approximately 1 cm^2 of surface area exposed. The coating process involved first polishing the electrodes using 600 grit metallurgical sandpaper followed by 1 micron diamond suspension for 15 minutes. Next, the electrodes were placed in a solution containing 7 g/L of $KMnO_4$ and 70 g/L H_2SO_4. The solution and electrode were maintained at 70°C in a heated water bath on a Fisher Isotemp hot plate in a fume hood. Following deposition, they were rinsed using deionized water.

2.2 CYCLIC VOLTAMMETRY

Cyclic voltammetry, a using an AUTOLAB PSTAT100 potentiostat, was done using a typical 3 electrode cell setup (Figure 2-1) in 600 mL of pH 10 NaOH solution prepared using NaOH (ACS grade, Fisher) and ultrapure water (Milli-Q Direct 16 Water Purification System, Millipore). The counter electrodes were graphite rods, and the reference electrode was Ag/AgCl/KCl(sat) (Broadly James, model Z113107). The starting potential and first vertex were 500 mV vs

Ag/AgCl/KCl(sat); the second vertex was 1200 mV. A scan rate of 20 mV/s was used, with a step size of 1.06 mV. The voltammogram was allowed to repeat until it traced over itself.

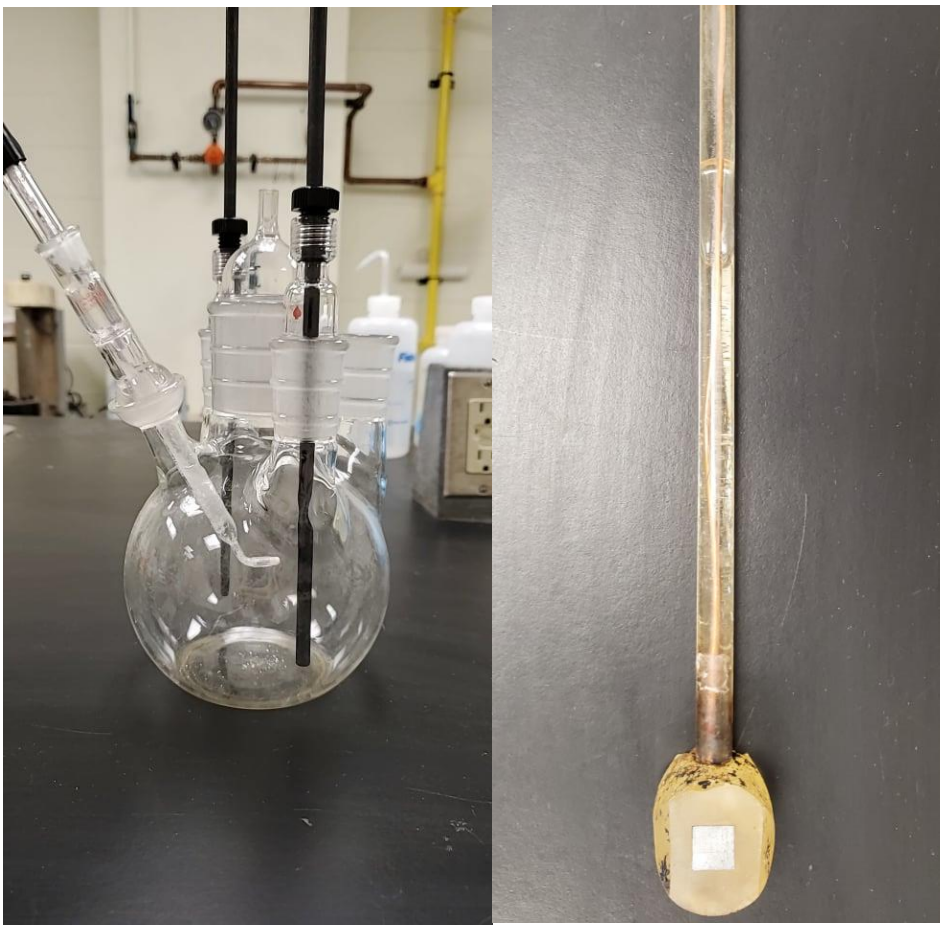

Figure 2-1: Three electrode cell (left) with carbon counter electrodes and reference electrode; 1 cm^2 lead working electrode (right).

2.3 RESULTS AND DISCUSSION

The voltammogram showed strong resistive behaviour with slight capacitive behaviour (see Figure 2-2). There was no evidence of oxygen evolution in the high potential region of the graph. Because of the strong resistive behaviour, using MnO_2 coated lead for electrolysis of

cyanide would require large voltages, as much of the power would be lost to overcoming the ohmic resistance of the electrode. For this reason, MnO_2 coated Pb electrodes were deemed unsuitable, and the focus of the thesis changed toward identifying a suitable alternative substrate material for coating with MnO_2.

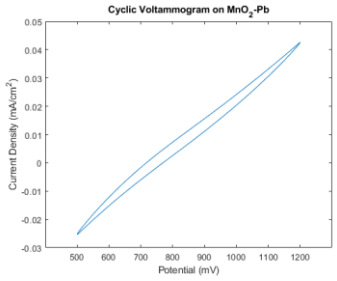

Figure 2-2: Cyclic voltammogram of MnO_2 coated Pb electrode in NaOH electrolyte, pH 10, between 500 mV and 1200 mV vs. satd. Ag/AgCl at a scan rate of 20 mV/s.

3 STAINLESS STEEL AS A SUBSTRATE

ANSI-304 stainless steel was selected as a possible suitable substrate for MnO_2 coating and cyanide destruction because it is a common and relatively cheap material of construction that is relatively stable under the caustic conditions required for oxidation of cyanide [21] (see Figure 3-1).

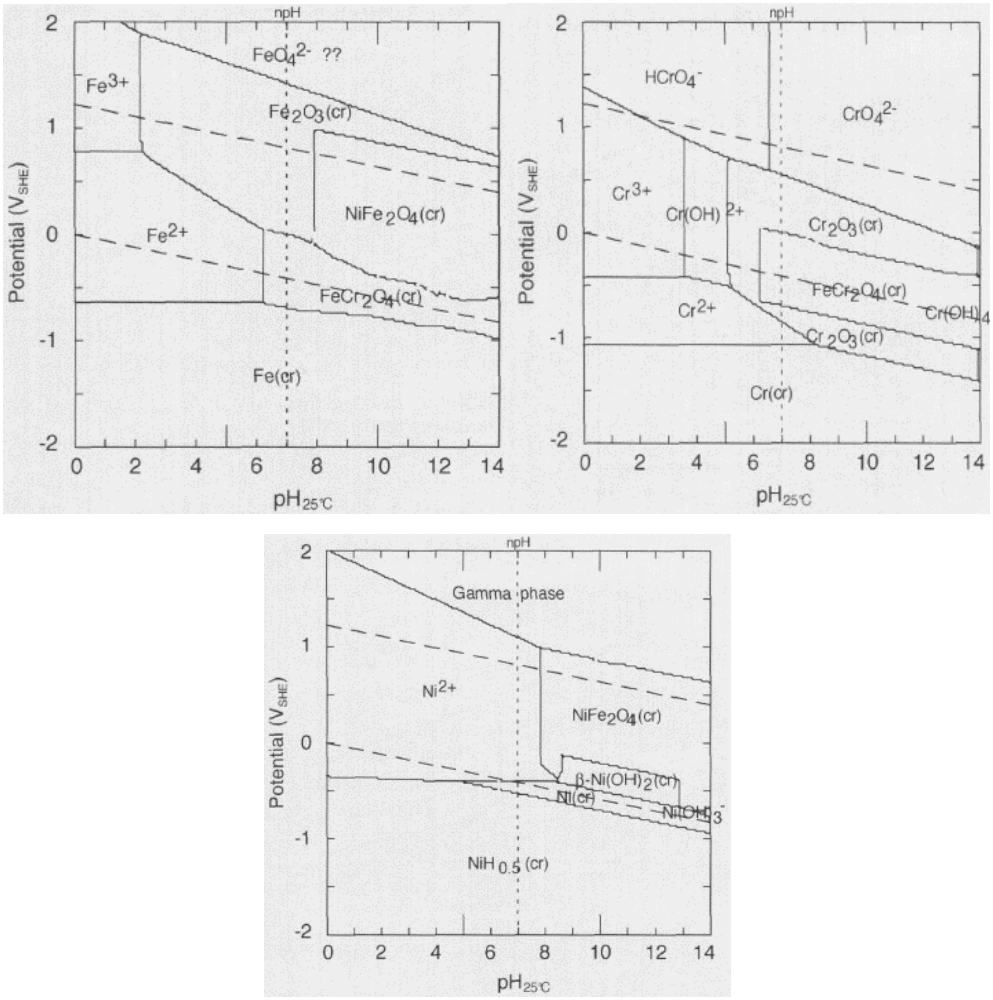

Figure 3-1: Pourbaix Diagrams for Fe (top left) Cr (top right) and Ni (bottom) in an aqueous system at 298 K, with dissolved activities = 10^{-6}, and p = 1 atm. Modified from [21].

Additionally, MnO_2 coated stainless steel substrates have shown promising electrochemical properties (Section 1.3.2), in particular for oxygen evolution.

3.1 STAINLESS STEEL IN CARBONATE SOLUTION

The first step in the evaluating the suitability of 304 stainless steel was to explore its stability at the pH and oxidizing potentials required for cyanide destruction. Due to the possible release of toxic HCN gas, carbonate was selected to act as a buffer to maintain a pH of 10. To achieve this target pH, a combination of sodium carbonate (ACS, Sigma-Aldrich) and sodium bicarbonate (ACS, Sigma-Aldrich) were added in a ratio of 2:3 for a total carbonate concentration of either 100 mM or 10 mM.

3.1.1 Methodology

Cyclic voltammetry was done using a similar 3 electrode cell setup using 600mL of pH10 carbonate buffered solution as previously described in Section 2.1 (Figure 2-1), either at a total carbonate concentration of 100 mM or 10 mM. The counter electrodes were graphite rods, and the reference electrode was Ag/AgCl/KCl(sat) (Broadly James, model Z113107). The starting potential and first vertex were -1200 mV vs Ag/AgCl/KCl(sat); the second vertex was 1500 mV. A scan rate of 100 mV/s was used, with a step size of 1.06 mV. The voltage was controlled using an AUTOLAB PSTAT100. The working electrode was cut from 5/8" ANSI-304 stainless steel rod (McMaster-Carr) to form a disc and sanded to 600 grit. The disc was inserted into an electrode holder (Figure 3-2) that had 1cm^2 of exposed area.

Figure 3-2: stainless steel working electrode with 1 cm^2 exposed area.

Measurements were sometimes difficult to reproduce due to oxygen bubbles forming on the working electrode causing hysteresis with the potential and current measurements. To address this, a set of cyclic voltammetry experiments was done using a rotating disc electrode (RDE) (Pine, AFMSRCE) at a rotation speed of 2800 rpm in order to transport dissolved oxygen away from the electrode surface and avoid bubble formation. The RDE was fitted with a 0.5 cm diameter disc that was lathed down from the same 304 stainless steel rod as previously described. The exposed area was 0.196 cm^2. The starting potential and first vertex were at 0mV; the second vertex was at 1500 mV. To minimize capacitive currents, a scan rate of 5 mV/s was used with a step size of 0.458 mV.

3.1.2 Results

Voltammograms of the bare stainless-steel electrodes in solutions buffered with 100 mM carbonate showed an oxidation current peak at approximately 1150 mV, just prior to the onset of massive oxygen evolution (see upper portion of Figure 3-3). This oxidative peak has been attributed to a transient dissolution/passivation process that is catalyzed by HCO_3^-/CO_3^{2-} , the peak current for which is directly proportional to the sodium bicarbonate concentration [22]. Although the process appeared quite reversible, by virtue of the lack of hysteresis in the voltammograms as the number of scans increased, the carbonate level in the electrolyte was lowered to 10 mM and the same cyclic voltammetry experiments were repeated. The resulting voltammograms (see lower portion of Figure 3-3) showed no unusual oxidation or capacitive currents in the region in question. From this it was determined that ANSI-304 stainless steel would likely be much less susceptible to corrosion in a 10 mM pH 10 carbonate buffer at

potentials near the onset of oxygen evolution. Hence, further experiments employed this lower carbonate concentration.

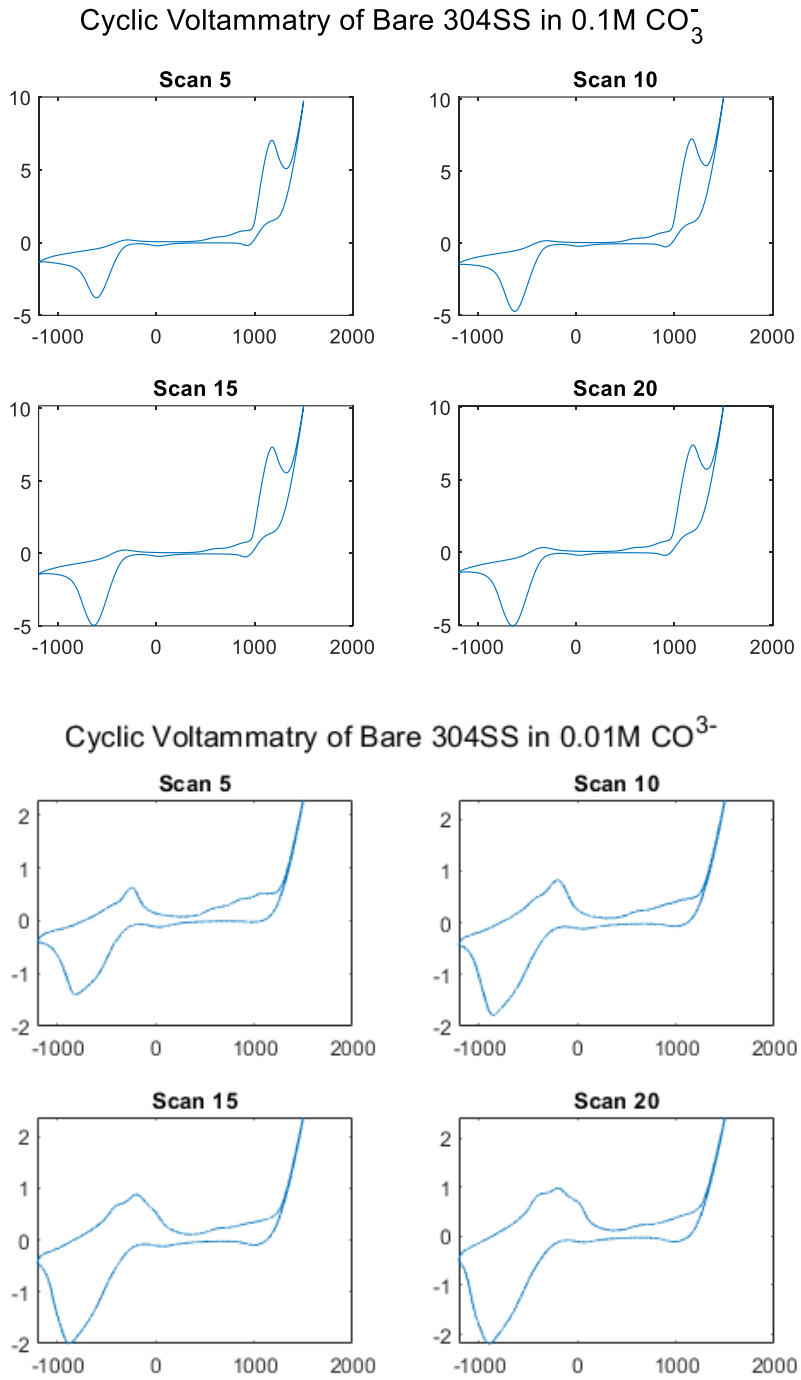

Figure 3-3: Cyclic voltammetry on bare ANSI-304 stainless steel in 10 mM CO_3^- (top) and 100 mM CO_3^- (bottom) between -1200 mV and 1500 mV vs Ag/AgCl/KCl(sat). Current density(mA/cm^2) on the vertical axis; potential (mV) on the horizontal axis.

3.2 MnO_2 COATINGS ON STAINLESS STEEL

The next phase of the research was to create a coherent and adherent MnO_2 coating on the 304SS substrate. The method for MnO_2 coating selected was detailed by Jacob and Zhitomirsky. [19] This technique was selected for ease of implementation, and because Jacob and Zhitomirsky reported that the technique produces a porous, crack free layer.

3.2.1 Methodology

Six 5/8" diameter 304 stainless steel discs were cut and polished as described in Section 3.1.1. Three of them were then coated with MnO_2. To apply the MnO_2 coating, an electrode was placed in a 0.1 M solution of $KMnO_4$ (ACS grade, Sigma-Aldrich) and a reducing current corresponding to -3mA/cm^2 was applied for 120 seconds. SEM-EDS (Jeol 6400 SEM, Oxford X-Max 80 EDS) analysis was employed to verify the 304 stainless steel composition and to verify that MnO_2 was successfully deposited on the electrodes.

3.2.2 Results

The chemical makeup of the bare 304 stainless steel samples was as expected (18%< Cr < 20%; 8% < Ni < 10.5%; remainder Fe) (see Table 3-1). The SEM imaging (see Figure 3-4) showed no notable surface features besides striations from sanding.

Table 3-1: Chemical makeup of 304SS surface measured through EDX.

Spectrum	Cr	Fe	Ni	Total
Mean (%)	19.79	71.89	8.32	100.00

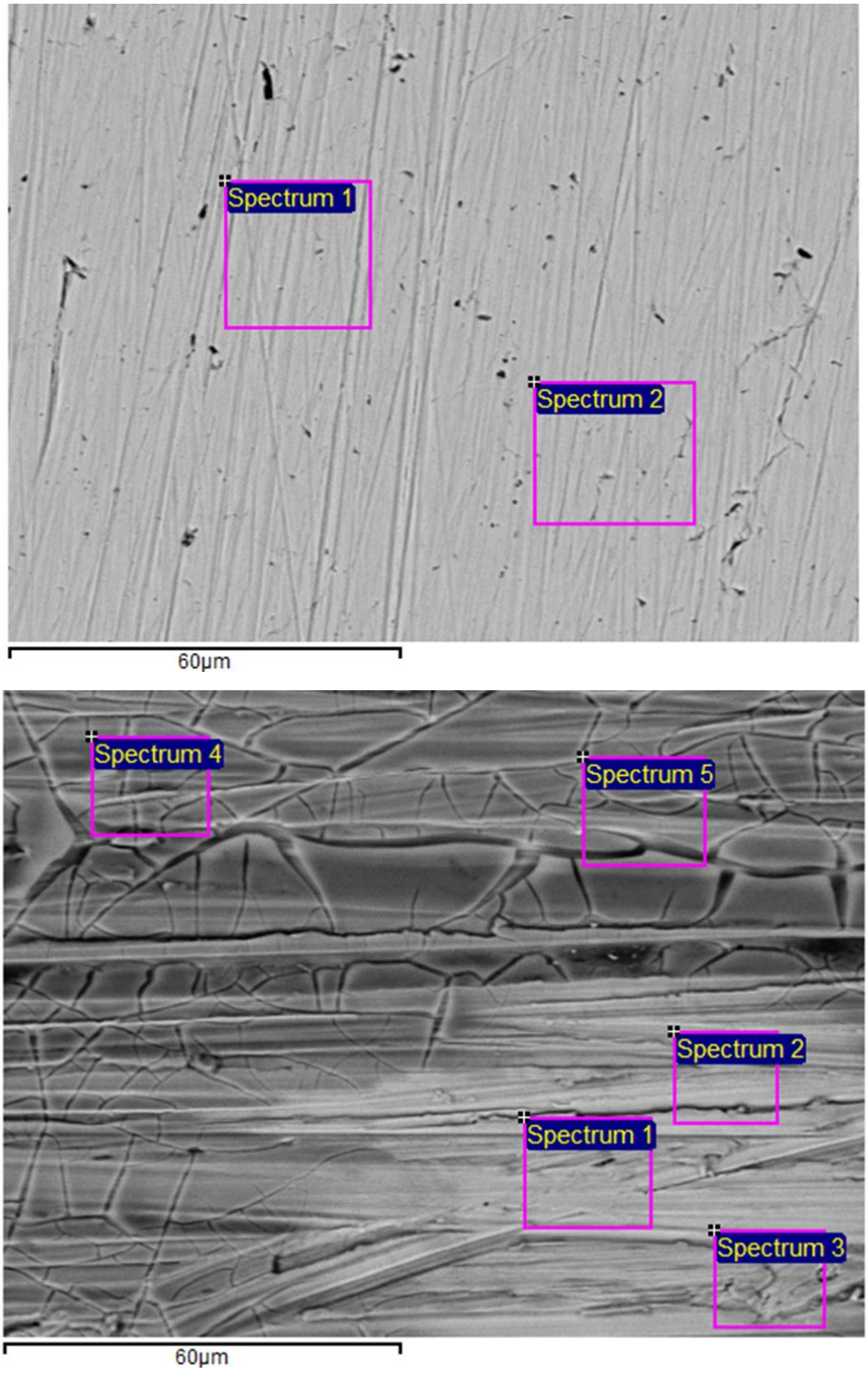

Figure 3-4: SEM image of 304SS (top) and MnO_2 coated 304SS (bottom); regions enclosed in boxes were sampled with EDS.

Conversely, the MnO_2 coated electrodes had several notable features. First, though Jacob and Zhitomirsky reported a crack-free layer, cracks can be seen in the surface of the MnO_2 deposit. However, these cracks appear to be superficial, possibly a result of drying too quickly. Second, on inspection a few regions lacked a complete deposit of the MnO_2 layer. Sporadically, approximate circles with low Mn content can be found. These regions were uncommon and are likely a result of the presence of gas bubbles on the electrode surface. Most electrodes showed no low Mn regions at all. Finally, a small amount of Na and K was measured, possibly indicating co-precipitation or entrapment of impurities during reduction to MnO_2.

Table 3-2: Chemical makeup of MnO_2 layer in 5 different regions of one sample; Spectrums 1-3 come from a partially coated region and are not representative of the majority of the layer.

Spectrum	Na	K	Cr	Mn	Fe	Ni	Total
Spectrum 1 (%)	0	0	19.32	2.55	70.70	7.43	100.00
Spectrum 2 (%)	0	0	19.14	2.98	70.18	7.70	100.00
Spectrum 3 (%)	0	0.44	18.36	6.09	67.30	7.81	100.00
Spectrum 4 (%)	1.77	1.77	16.02	17.36	56.78	6.31	100.00
Spectrum 5 (%)	1.45	1.60	16.35	16.35	58.05	6.20	100.00

3.3 ELECTROCHEMICAL CHARACTERIZATION OF BARE AND MnO_2 COATED 304SS

The suitability of bare and MnO_2 coated 304 stainless steel electrodes for cyanide oxidation was studied using cyclic voltammetry.

3.3.1 Methodology:

Cyclic voltammetry was performed on both bare and MnO_2 coated 304 stainless steel electrodes using the same cell setup as described in Section 3.1.1. The starting potential and first vertex were at 0 mV; the second vertex was at 1500 mV. To minimize capacitive currents, a

scan rate of 5 mV/s was used with a step size of 0.458 mV. The RDE was assembled as described in Section 3.1.1 using a 0.5 cm diameter 304 stainless steel disc, with 0.196 cm^2 of exposed area.

3.3.2 Results

At and beyond 1000 mV, the CVs for MnO_2 coated steel were similar to the bare 304 stainless steel (See Figure 3-5). Both show oxygen evolution starting around 900 mV vs Ag/AgCl/KCl(sat) and exhibit similar current densities. The major difference is the capacitive behaviour of the MnO_2 layer at lower potentials. The high capacitance of the MnO_2 layer is consistent with reporting from Jacob and Zhitomirsky [19]. Importantly, there are no identifiable faradaic currents, so MnO_2 coated 304 stainless steel was tentatively accepted as stable at oxidizing potentials in 10 mM carbonate solution at pH 10.

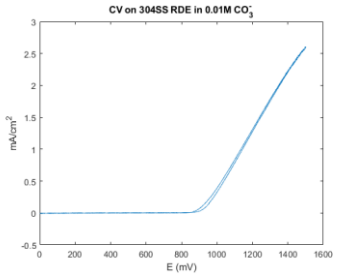

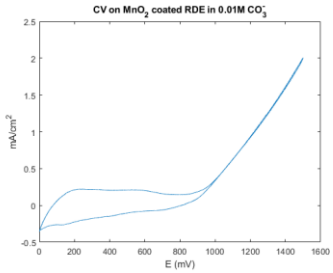

Figure 3-5: Cyclic voltammetry on bare (top) and MnO2 coated (bottom) ANSI-304 stainless steel in 10mM CO_3^- between 0mV and 1500mV vs Ag/AgCl/KCl(sat) using a rotating disc electrode at a rotation speed of 2800 rpm. Current density(mA/cm^2) on the vertical axis; potential (mV) on the horizontal axis.

4 CYANIDE OXIDATION ON BARE AND MnO_2 COATED 304 SS ELECTRODES

Having characterized the bare and MnO_2 coated 304 stainless steel electrodes in cyanide free electrolytes, the next phase of the research program was to add cyanide to the electrolyte and explore their potential use for oxidation of cyanide. This was done, first, using cyclic voltammetry and frequency response analysis to explore the changes in electrochemical behavior of the electrodes as the electrolyte was spiked with increasing concentrations of cyanide. The experiments were followed by a series of galvanostatic experiments in which the cyanide concentration was analyzed as a function of time from a fixed starting concentration.

4.1 CYCLIC VOLTAMMETRY

Cyclic voltammetry was used to ascertain the potential at which cyanide is destroyed on bare and MnO_2 coated 304 stainless steel. In general, a baseline (cyanide free) voltammogram was established, and the cyanide concentration was increased in stages by spiking the electrolyte a small volume of a concentrated cyanide solution and the cyclic voltammetry procedure was repeated. This process was then repeated at increasing cyanide concentrations.

4.1.1 Methodology

Cyclic voltammetry was done using an AUTOLAB PSTAT100 with a typical 3 electrode cell setup with 600 mL of pH 10, 10mM carbonate (cyanide free) electrolyte, as previously described in Section 3.1.1. The counter electrodes were graphite rods, the reference electrode was Ag/AgCl/KCl(sat), and the working electrode was a rotating disc electrode with 0.196 cm^2 of exposed electrode surface as previously described in Section 3.1.1. An electrode rotation speed of 2800 rpm was used. The starting potential and first vertex was 250 mV vs Ag/AgCl/KCl(sat); the second vertex was 1750 mV. A scan rate of 100 mV/s was used, with a

step size of 1.06 mV. After every 10 cycles, 3mL of concentrated cyanide was spiked into the cell, using a mechanical pipette (vwr, 100-1000 uL) increasing the cyanide concentration by 50 ppm, and the voltammetry procedure was repeated. The concentrated cyanide solution was prepared using 3.6 g of NaCN in 200 mL of ultrapure water (Milli Q Direct 6 System, Millipore).

4.1.2 Results

Both the MnO_2 coated and bare steel electrodes exhibited evidence of mass transfer limited cyanide oxidation at potentials near the onset of oxygen evolution. As cyanide

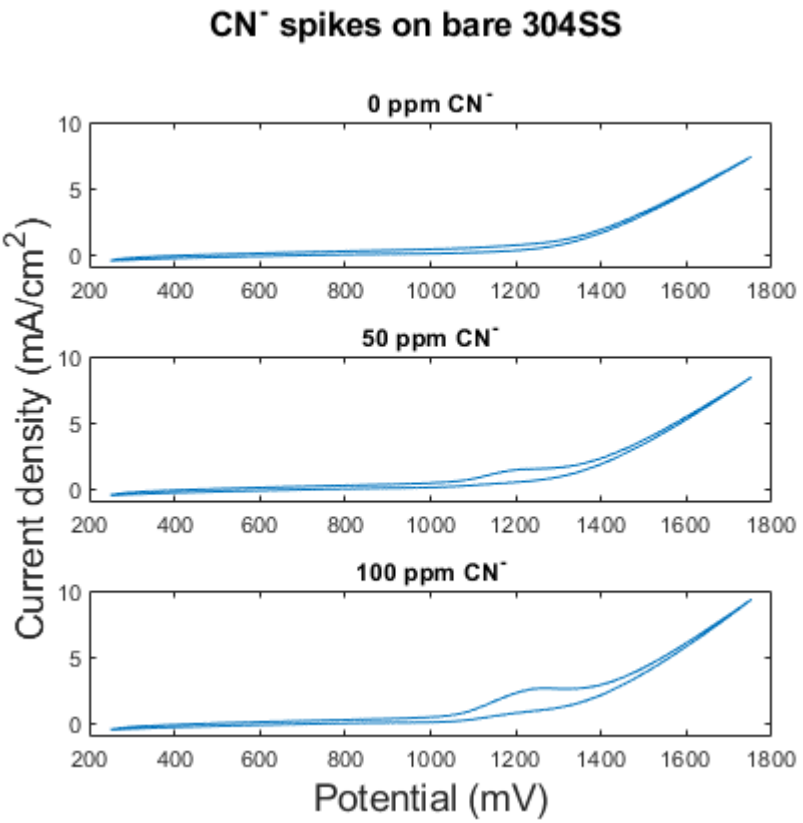

Figure 4-1: cyclic voltammetry on bare ANSI-304 stainless steel in 10mM CO_3^- between 250mV and 1750mV vs Ag/AgCl/KCl(sat) using a rotating disc electrode at a rotation speed of 2800 rpm with 0ppm CN^- (top), 50ppm CN^- (middle), and 100ppm CN^- (top). Current density(mA/cm^2) on the vertical axis; potential (mV) on the horizontal axis.

concentration increases, a peak is seen growing at ~1200 mV vs Ag/AgCl (see Figure 4-1 and 4-2), at the onset of oxygen evolution.

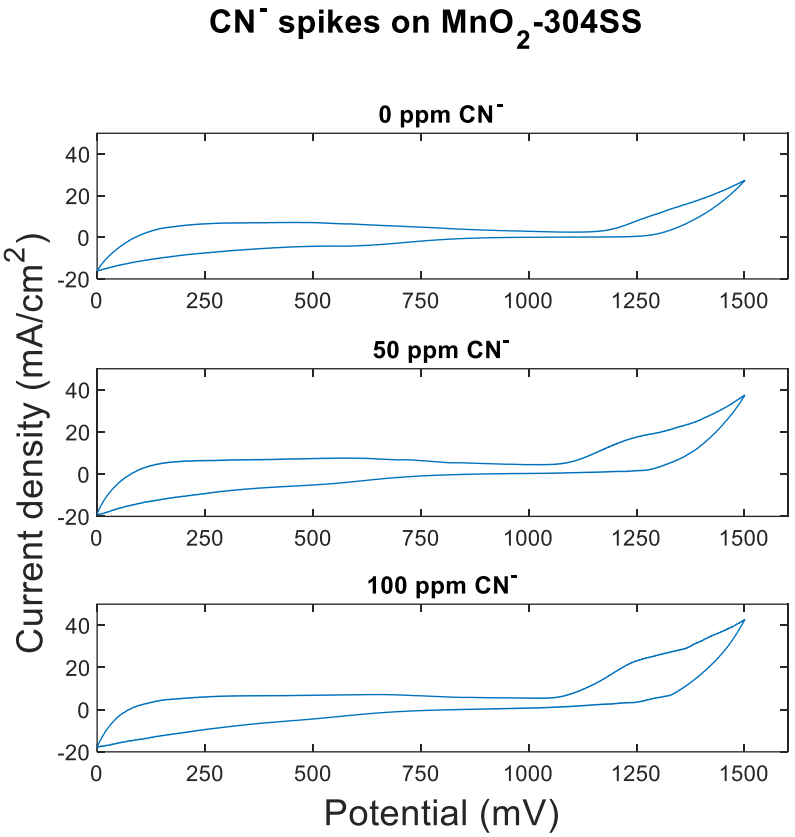

Figure 4-2: cyclic voltammetry on MnO_2 coated ANSI-304 stainless steel in 10mM CO_3^- between 250mV and 1750mV vs Ag/AgCl/KCl(sat) using a rotating disc electrode at a rotation speed of 2800 rpm with 0ppm CN^- (top), 50ppm CN^- (middle), and 100ppm CN^- (top). Current density(mA/cm^2) on the vertical axis; potential (mV) on the horizontal axis.

These results are in-line with general mechanism put forward by Comninellis [14], namely that electrolytic oxidation of organic species occurs by its reaction with adsorbed hydroxide radicals that are formed as precursor to oxygen evolution. More specifically, the nature of the oxygen radical species where cyanide is oxidized on 304 stainless steel might be $Ni(OH)_3$ [13], by virtue of the nickel content in 304 stainless steel, which is ca. 8% by weight. Additionally, the

MnO_2 coated electrode shows higher currents overall. This is at least partially due to the larger capacitive currents, but may also be a result of solid state charge transfer reactions corresponding to $MnO_2/Mn_2O_3/Mn_3O_4/MnO$ transformations (as indicated in the Eh-pH diagram in Section 1.3) within the electrode surface.

4.2 GALVANOSTATIC CYANIDE DESTRUCTION

With evidence of mass transfer limited cyanide destruction at the onset of oxygen evolution, the next step was to apply a fixed current and track the fractional cyanide destruction over time. In general, two sets of galvanostatic experiments were performed; one which explored various current densities over a fixed period, and another set that explored the effect of time at a fixed current density. The motivation for first set of experiments was to ascertain which applied currents would be most effective for cyanide destruction. The logic being that once cyanide destruction reaches the mass transfer limiting rate, larger currents are a waste of power, as those currents will only contribute to oxygen evolution instead of cyanide destruction. The second set of experiments was undertaken to explore the kinetics of cyanide oxidation in order to extract kinetic parameters that could be used to design an industrial electrolytic cyanide oxidation process. The effect of dissolved copper as a catalyst for cyanide oxidation was also explored.

4.2.1 Methodology

Cells were built using 400 mL beakers containing 350 mL of electrolyte and topped with a PVC lid in which slots had been milled in order to hold the electrodes parallel and at a uniform distance of 6.5 cm apart (Figure 4-3). The electrolyte was 471 mg/L CN^- , prepared by dissolving

1.13 grams of NaCN (ACS, Anachemia) in 10 mM pH 10 carbonate buffer solution. The anode and cathode were both manufactured from 4" x 1/8" 304 stainless steel plate (McMaster-Carr); the anode was either bare or coated with MnO_2, as described in Section 4.1.1. The cathode area was 4cm×6.5cm; the anode has the same dimensions, but the edges, back, and top of the anode were covered using electroplating tape (470, 3M), restricting the exposed area to 4 cm x 5 cm. This was done to keep the exposed area consistent between anodes, as the actual construction of the electrodes had some small variation in dimension. A DC power source (Heathkit, IP-28) was used to apply a variety of current densities between 1 mA/cm^2 and 6 mA/cm^2. The currents were applied for either 6, 12, or 24 hours. To keep the test conditions consistent and perform multiple experiments simultaneously, the cells were arranged in series. Voltages across each the cells were recorded at a sample rate of 50 Hz using two USB-6009 National Instruments DAQ cards using differential analog inputs. To make agitation consistent

across cells, up to six cells at a time were arranged on a multiplate stirrer (Labline Multi Magnestir) to be moderately agitated using PTFE coated magnetic stir beads.

When copper was added to the electrolyte, it was done so at a concentration of 10 mg/L Cu^{2+}, introduced as 24 mg/L $CuSO_4$, added to the electrolyte by addition of a 1 mL spike. The residual cyanide concentration was measured using titration with a $AgNO_3$ standard according

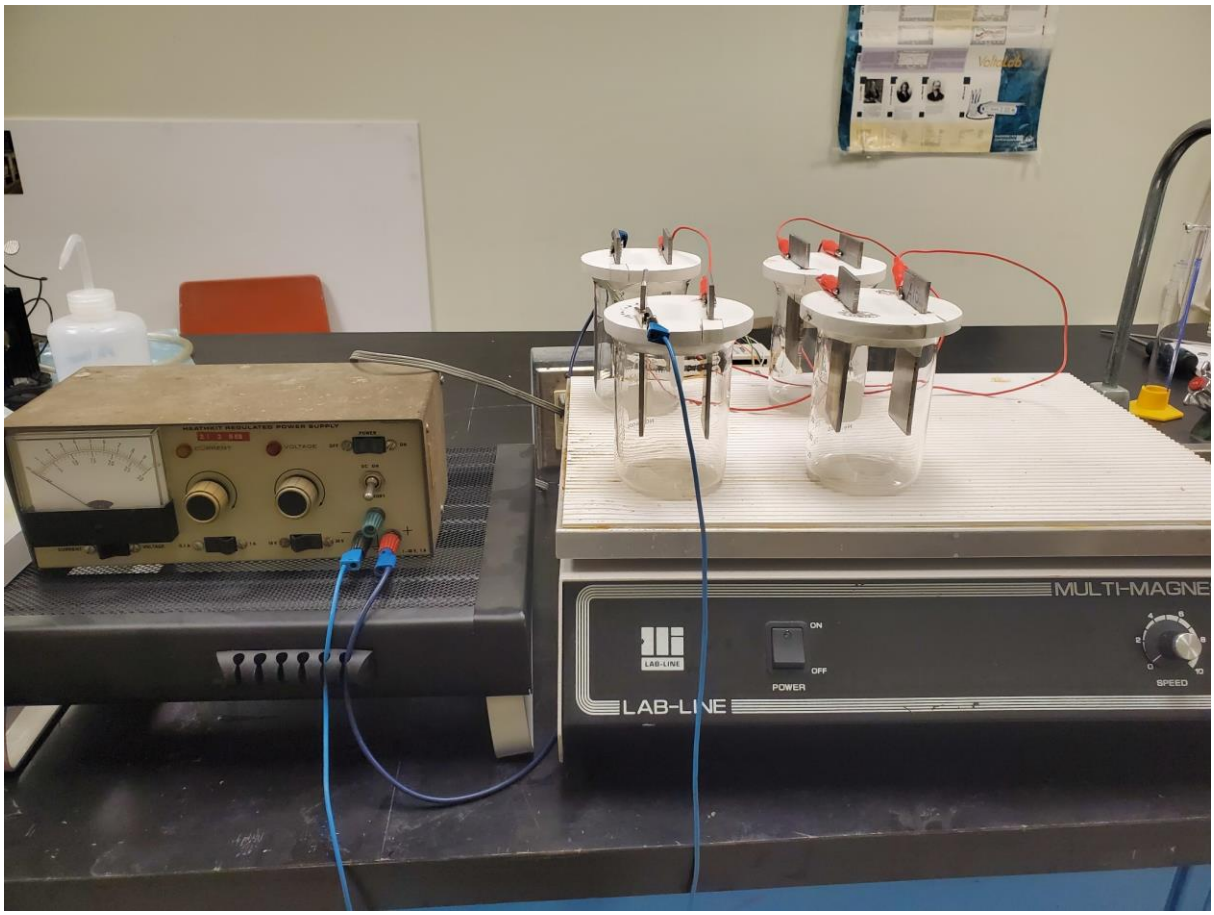

Figure 4-3: Four galvanostatic cells in series.

to the procedure described by Breuer et al [23]. $AgNO_3$ titrants were prepared by mixing 4.12 g of $AgNO_3$ in 200 mL of ultrapure water (Milli-Q Direct 16 Water Purification System, Millipore).

Selected samples of electrolyte were sent to an external laboratory (Perdue Central Analytical Facility) for ICP-MS analysis (see Appendix 2). A wide range of metal content was analyzed, but of particular interest were Fe, Ni, and Cr (as evidence of steel leaching into solution), Mn (as evidence of MnO_2 layer degradation), and Cu (to track Cu concentration over the course of electrolysis). Solution samples were prepared for analysis by first pouring them into 50 mL centrifuge tubes. A large excess of solid $AgNO_3$ was then added to the electrolyte to oxidize any remaining cyanide. The samples were then centrifuged for 2 hours. 5 mL of the clarified solution was then transferred via mechanical pipette (VWR, 100-1000uL) to another centrifuge tube and diluted to 50 mL using 1% HNO_3 prior to being sent out for analysis.

4.2.2 Results

An applied current density of 2 mA/cm^2 had the greatest effect on lowering residual cyanide concentration after 24 hours. Counterintuitively, larger current densities of 4 mA/cm^2 and 6 mA/cm^2 performed worse. This might be because the larger voltages required to drive the current further promoted oxygen evolution over cyanide oxidation. Additionally, the larger currents corroded the electrodes, caused a visible orange discoloration of the surface and a visible orange tint in the electrolyte, consistent with the formation of iron hydroxide precipitates. The mechanism of iron corrosion is unknown, but the iron solutes may have formed a complex with the free cyanide, forming weak acid dissociable (WAD) cyanide. Based on these results, further experiments were conducted at 2 mA/cm^2 in order to minimize stainless steel corrosion. The introduction of copper might have reversed the pattern of larger currents performing worse, as copper is catalytic for WAD cyanide destruction, but the high potentials required to drive the higher currents and the visible anode degradation were

deemed too costly.

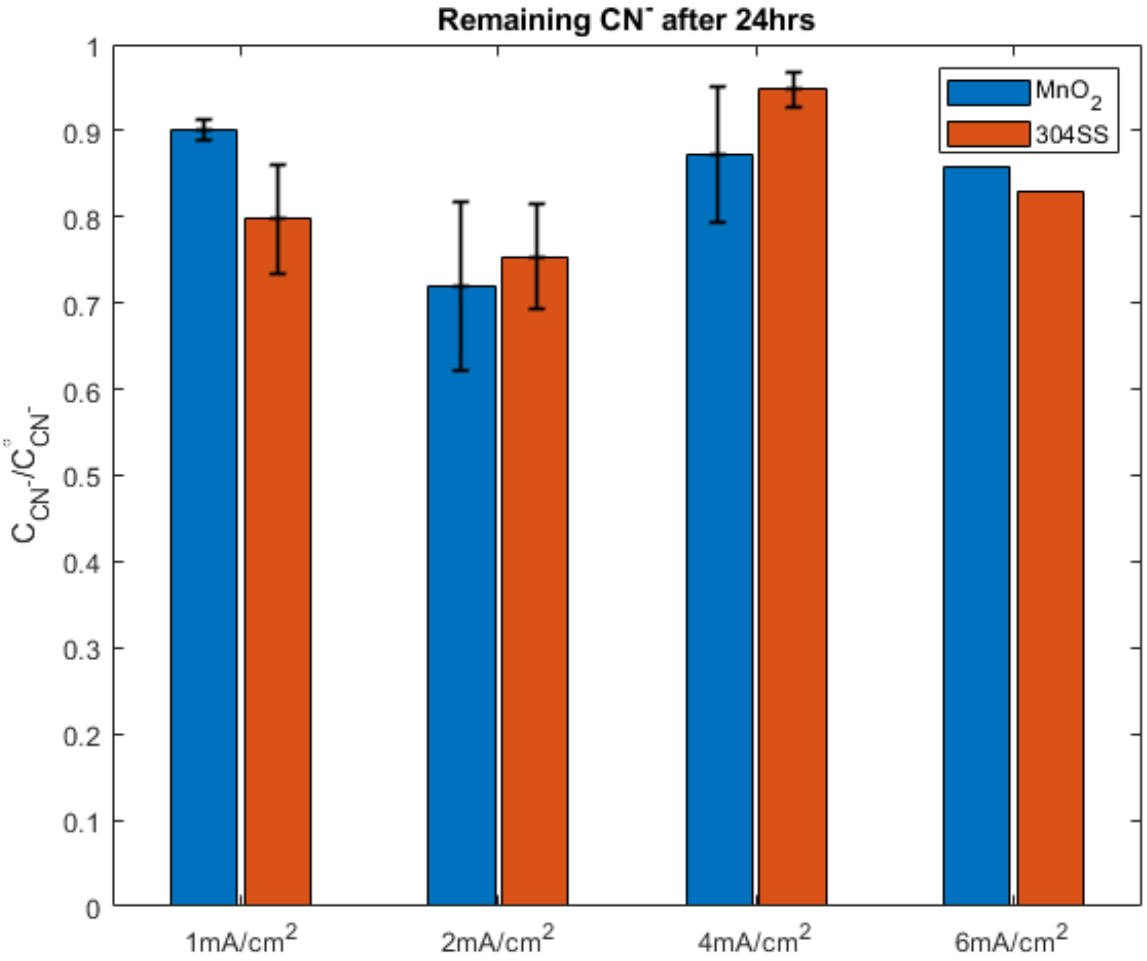

Figure 4-4: Remaining cyanide concentration (±SD) after 24hrs of applied current; the 6mA/cm^2 lacks error bars as it was only performed once.

Experiments at a current density of 2 mA/cm^2 were done for varying time lengths; 6, 12, or 24 hours. The electrolyte pH was measured before and after electrolysis and showed no significant drift. The residual cyanide concentration was fitted to an exponential decay model, Equation 4-1, corresponding to first order mass transfer limited kinetics. The resulting 'k' values, resulting from a least-squared fit of the results for the various experiments are presented in Table 5-1

along with average cell voltages and overall current efficiency values, calculated on the basis of oxidation of CN^- to CNO^- according to Equation 1-8.

$$C_{CN^-}(t) = C^{\circ}_{CN^-} e^{-\frac{A}{V}kt} \qquad 4\text{-}1$$

Table 4-1: geometry independent rate constants (cm/hr, top), average current efficiency (bottom), and average voltage for galvanostatic cyanide oxidation at 2mA/cm².

$\boldsymbol{k}$(cm/hr)	Without Copper	With Copper
Bare Steel	0.254	1.406
MnO_2-304SS	0.247	0.270
$\boldsymbol{\phi}$		
Bare Steel	2.6%	8.1%
MnO_2-304SS	2.3%	2.7%
$\boldsymbol{E(V)}$		
Bare Steel	4.57	4.43
MnO_2-304SS	4.25	4.37

As illustrated in Figure 4-5, without the presence of copper, both the MnO_2 coated anodes and bare steel anodes performed similarly, albeit relatively poorly. The cells perform better when copper is introduced to the electrolyte (as illustrated in Figure 4-6). Against expectation, the improvement for MnO_2 coated electrodes is very modest, while the improvement for bare steel is significant. With copper present, the reaction kinetics fit the exponential decay model much better.

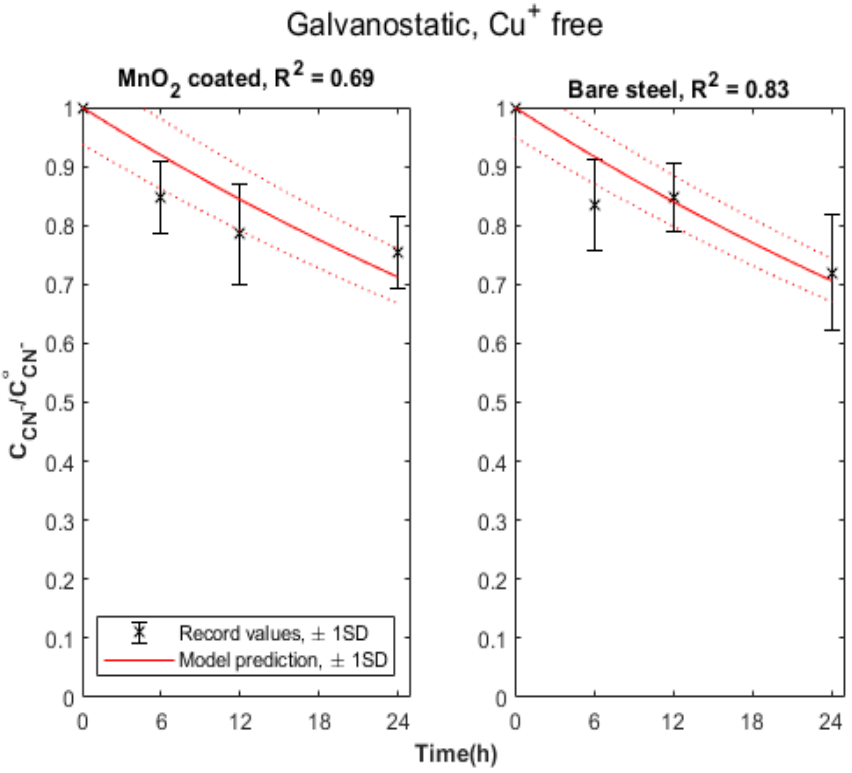

Figure 4-5: Cyanide concentration decay (black) from 2 mA/cm^2 current over time in a copper free environment; in red is a fitted exponential decay model.

To try to understand the role of copper on the relative performance for cyanide oxidation kinetics between bare 304 stainless steel and MnO_2 coated stainless steel, the copper concentrations, from ICP-MS analysis, were plotted as a function of time (see Figure 4-7). Of note is that after 6 and 12 hours the cells with bare steel electrodes showed higher copper concentrations in the electrolyte relative to the cells with MnO_2 coated electrodes. The lower copper concentrations in the cells with MnO_2 coated electrode may have resulted from copper(I) oxidation at the electrode surface that resulting in the formation of stable Mn-Cu-O oxides, similar to those reported by Wei et al [23], which removed copper from solution and negated its catalytic effect. This explanation is consistent with the observed similar performance between copper free and copper containing electrolytes in cells equipped with

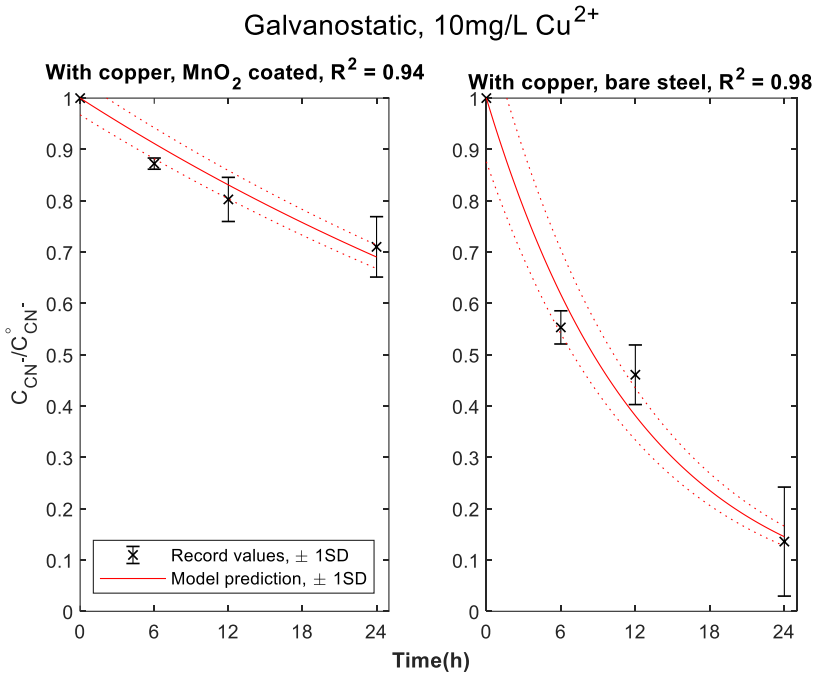

Figure 4-6: Cyanide concentration decay (black) from 2mA/cm² current over time in the presence of copper; in red is a fitted exponential decay model

MnO_2 coated electrodes. Conversely, copper(I) oxidation at the bare stainless steel electrode likely resulted in the formation of copper hydroxide:

$$[Cu(CN)_3]^{2-} + 8OH^- \rightarrow Cu(OH)_2 + 3CNO^- + 3H_2O + 7e^- \qquad 4\text{-}2$$

These copper precipitates were likely loosely adherent and largely ejected from the surface by the action of the evolving oxygen gas bubbles where they redissolved in the bulk electrolyte. In this regard, Wels and Johnson [11] describe the dissolution of CuO as being enhanced by increasing cyanide concentration and transport of cyanide ions according to the following equation:

$$CuO + 4CN^- + H_2O \rightarrow [Cu(CN)_4]^{2-} + 2OH^- \qquad 4\text{-}3$$

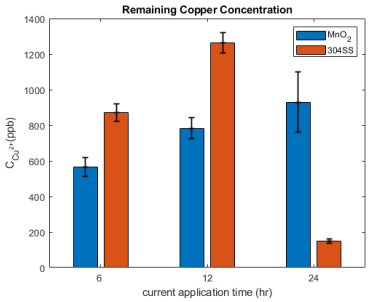

Figure 4-7: residual copper concentration after 6, 12, and 24 hours of 2 mA/cm^2 current applied to pH 10, 250 ppm CN^-solution in 10mM carbonate.

The cupric cyanide generated by the above reaction would then be expected to oxidize cyanide to cyanate as previously described in Section 1.1.1. This would help explain the observed improvement of cyanide oxidation kinetics for copper containing electrolytes in cells equipped with bare stainless steel electrodes relative to cells equipped with MnO_2 coated electrodes.

The collapse of copper concentration after 24 hours, in the electrolyte from the cells equipped with bare stainless steel electrodes is likely due to precipitation of copper oxide. This result was expected, to an extent. Cyanide has a stabilizing effect on copper. As cyanide is destroyed, there is less of it available to complex with copper and the free copper concentration increases. This pattern continues until there is insufficient cyanide left to stabilize

the copper at all, and the copper precipitates. In this regard, the precipitation of copper hydroxides is known to occur at low cyanide concentration during the final stages of the INCO SO_2/Air process [9].

The electrodes showed some evidence of degradation in the form of elevated nickel, chrome, and iron concentrations in the electrolyte over time (see Appendix 3). In general degradation in presence of copper was significantly worse than without copper present. MnO_2 coated electrodes showed less overall steel degradation compared to bare steel but did show manganese in solution after 24 hours of electrolysis, indicating the MnO_2 layer itself degrading.

4.3 IMPLICATIONS FOR GOLD ELECTROWINNING

Cyanide oxidation is observed in gold electrowinning from gold cyanide liquors [2] [3] . The conditions of this experiment are similar to those of gold electrowinning, suggesting that cyanide may be oxidized at the mass transport limiting rate. These results may allow for the prediction of the total rate of cyanide loss, which is important for replacing lost cyanide in the event the leach solution is recycled. There are several limitations to the application of these results: gold electrowinning is typically conducted at greater pH and temperature (which may impact the transport properties of cyanide ions) and greater currents (which may produce greater micro-convective transport of cyanide to the electrode surface through greater rates of oxygen bubble formation). These results also suggest that copper in the electrowinning electrolyte must be kept to a minimum.

5 CELL DESIGN

The results of the galvanostatic experiments were used to inform the design an electrolytic cyanide destruction cell and evaluate its feasibility for industrial application. Figure 5-1 shows a thin slice of a mass transfer limited flow cell, where v is the volumetric flowrate and A^* is the anodic area of the slice. Equation 5-2 shows the solution to the resulting differential equation where w is the spacing between the cathode and anode, V is the volume of the flow cell, A is the total anode area in the cell, L Is the total cell lengths, and τ is the mean residence time. It is useful to measure the flow cell size in "unit cells" of a specific area, $\dot{A}$.

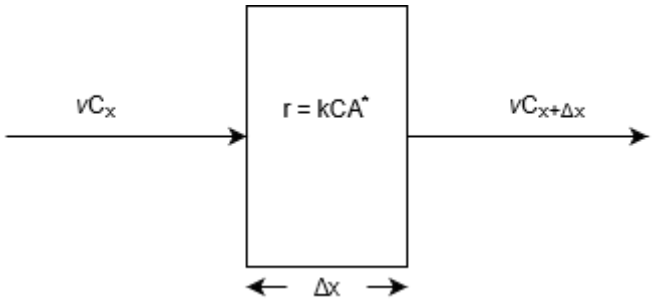

Figure 5-1: thin section of a mass transfer limited electrolytic flow cell

$$\frac{dC(x)}{dx} = -\frac{kC(x)h}{v} \qquad 5\text{-}1$$

$$C(L) = C^{\circ}e^{\frac{-kA}{v}} = C^{\circ}e^{\frac{-kA\tau}{V}} = C^{\circ}e^{\frac{-k\tau}{w}} \qquad 5\text{-}2$$

$$C(N) = C^{\circ}e^{\frac{-kN\dot{A}}{v}} \qquad 5\text{-}3$$

Equation 5-3 can then be used to model a set of N unit flow cells in series.

5.1 POWER EFFICIENCY

The current efficiency of the cell is given by Equation 5-4, where i is the current density, while Equation 5-5 follows from Equation 5-3.

$$\phi = \frac{i}{i_{tot}} \qquad 5\text{-}4$$

$$i(N) = nFr(N) = nFkC(N) \qquad 5\text{-}5$$

Using the first order kinetics model, the current efficiency can be established over the range of the electrolysis. The average current efficiency can be found through the mean value theorem. This is equivalent to the ratio of the total charge transfer across the anode vs charge transfer associated with cyanide oxidation. Immediately apparent is the drop in average current efficiency the longer the cell becomes. The current efficiency will be greater at earlier stages of electrolysis due to greater transport of cyanide to the anode surface.

$$\bar{\phi} = \frac{1}{Li_{tot}}\int_0^L idx = \frac{1}{Ni_{tot}}\int_0^N idN = \frac{nFk}{Ni_{tot}}C^\circ\left(1 - e^{\frac{-kN\dot{A}}{v}}\right) \qquad 5\text{-}6$$

$$\lim_{N\to 0}\bar{\phi} = \frac{nFk}{i_{tot}}C^\circ$$

$$\lim_{N\to\infty}\bar{\phi} = 0$$

5.2 REACTOR SIZING AND POWER COSTS

The required size of the reactor, and associated capital and operating costs were estimated.

5.2.1 Capital costs for the electrolytic flow cell

Since cyanide electrolysis is not currently done in industry, data for capital costs does not exist. However, copper electrowinning cells feature similar characteristics to the electrolysis cell described above, using similar materials of construction (steel-based electrodes), and

operating at similar temperatures, flow rates, and voltages. For these reasons, capital cost estimations for a copper electrowinning plant were used as the basis for capital cost of similar sized cyanide electrolysis plant. The major differences are the current densities and electrolyte pH. Copper electrowinning is done under acidic conditions and roughly 300 A/m^2, while the cyanide electrolysis described in Section 5 is done at 20 A/m^2 in alkaline conditions. Additionally, a cyanide electrolysis plant may require more safety considerations, in particular more aggressive ventilation to mitigate potential cyanide off gases. The capital cost estimations should, therefore, be considered optimistic. The capital cost estimation is given in Equation 5-7 in USD [24], and is valid between 14 and 975 unit cells with an area of 30 m^2.

$$Capital\ Cost = \alpha(N)^{\beta} \qquad 5\text{-}7$$

$$\alpha = 379000$$

$$\beta = 0.971$$

$$\dot{A} = 30m^2$$

5.2.2 Operating costs

The primary operating costs of an electrowinning cell are the power requirements, replacement of electrodes, and replenishment of reagents. In the case of electrolysis of cyanide, there are no reagents to replenish, and electrodes would need to be replaced at a considerably lower rate. The primary operating cost of concern is therefor the power costs. For this report, a power cost of 0.085 USD/kWh will be assumed, based on the average global adjustment price reported by the Independent Electricity System Operator (IESO) of Ontario in 2019. The operating power cost can then be described by Equation 5-8, where P is the power cost factor and E is the voltage.

$$power\ cost = Pi_{tot}\dot{A}NE \quad (5\text{-}8)$$

The average voltage required to drive the 20A/m^2 current in the cells described in Section 5 was 4.5 volts. However, a portion of the voltage is unrelated to the chemical reactions and simply due to electrolyte resistance.

$$E = E_{anode} - E_{cathode} + IR \quad (5\text{-}9)$$

The voltage caused by can be mitigated by minimizing the gap between electrodes. The electrolyte resistance between two electrodes follows Equation 5-10, where σ is the electrolyte specific conductivity.

$$IR = i_{tot}\frac{l}{\sigma} \quad (5\text{-}10)$$

The specific conductivity for the cyanide bearing carbonate electrolyte used is 0.0054 S/cm [25]. At an electrode spacing of 6.5 cm and a current density of 0.002 A/cm^2, the IR voltage is estimated to be 2.4 V. Hence, the required voltage required to drive the reactions, $E_{anode} - E_{cathode}$, is only ca. 2.1 V (4.5 V – 2.4 V). The overall voltage of the cell can be significantly reduced by reducing the electrode gap. For example, an electrode gap of 2 cm, would be predicted to result in an overall cell voltage of 2.8 V, based on a corresponding estimated IR drop of 0.7 V. It is assumed that the pH 10 cyanide bearing carbonate solution has a comparable conductivity to that of the waste effluent stream in industry, which is primarily cyanide and NaOH.

5.2.3 Flow cell size for total conversion

To meet environmental regulation for residual cyanide, the reaction needs to proceed until a final concentration of 1 ppm has been reached, as specified by Canadian federal

regulation [5]. The corresponding required reactor size, N, can be determined by Equation 5-11.

$$N = -\frac{v}{k\dot{A}} ln\left(\frac{1ppm}{C^\circ}\right), \textit{ in terms of } N \qquad 5\text{-}11$$

$$A = -\frac{v}{k} ln\left(\frac{1ppm}{C^\circ}\right), \textit{ in terms of total area}$$

Table 5-1 shows the required area and unit cells of 30m^2 for flowrates between 5000m^3/day and 40000m^3/day using a stainless-steel anode as described in Section 5.

Table 5-1: flow cell sizes required for regulation sufficient conversion of cyanide.

v m^3/day	5000	10000	15000	20000	25000	30000	35000	40000
v m^3/hr	208	417	625	833	1042	1250	1458	1667
A m^2	81814	163628	245442	327256	409070	490884	572698	654512
N	2727	5454	8181	10909	13636	16363	19090	21817

On inspection, these values for number of reactors and electrode area are infeasible. They are orders of magnitude greater than those of similar processes in industry. [24] However, this result is partly since the instantaneous current efficiency drops over the course of electrolysis. It is possible that this technology might be cost efficient if it were to be applied as a first stage of cyanide oxidation followed by a convention chemical oxidation process as a polishing stage.

5.3 ELECTROLYSIS AND INCO SO_2/AIR IN SERIES

If the flow cell does not sufficiently destroy the cyanide, the remainder must be dealt with using conventional chemical methods. In 2010, INCO reported they spent between 1.22 USD and 4.5 USD per kilogram of cyanide destroyed using their process, primarily due to chemical costs and varying concentrations of cyanide. For this report, values of 1.22 USD/kg as

a best case and 2.86 USD/kg as a median case will be considered. Where Q is the variable reagent cost factor:

$$Reagent\ Cost = vC^{\circ}_{CN^-}Q \text{ , without electrolysis} \quad 5\text{-}12$$

$$Reagent\ Cost = vC_{CN^-}(N)Q, \text{ after } N \text{ stages of electrolysis}$$

$$Cost\ Savings = vC^{\circ}Q\left(1 - e^{\frac{-k\dot{A}N}{v}}\right) - Pi_{tot}\dot{A}NE \quad 5\text{-}13$$

After T years of operation for a capital cost R, combining Equations 5-7 and 5-13:

$$NPV(N,T) = \left[vC^{\circ}Q\left(1 - e^{-\frac{k\dot{A}N}{v}}\right) - Pi\dot{A}NE\right]\left(\frac{1-(1+R)^{-T}}{R}\right) - \alpha(N)^{\beta} \quad 5\text{-}14$$

5.3.1 Maximum cost savings

The local optima of Equation 5-13 can be found by setting the derivative to 0.

$$kQC^{\circ}e^{\frac{-k\dot{A}N}{v}} - Pi_{tot}E = 0 \quad 5\text{-}15$$

Equations 5-4 and 5-5 can then be reintroduced. The instantaneous current efficiency at the point of greatest cost savings follows Equation 5-16.

$$\phi(N) = \frac{PEnF}{Q} \quad 5\text{-}16$$

Intuitively, the target current efficiency after N cells can be understood as the ratio between the cost of one mole of oxidizing reagents to the cost of one mole worth of charge transfer across the anode. Notably, the target current efficiency is independent from electrode area, flow rate, or initial concentration. Instead, those values will all impact the number of unit cells required to achieve the target efficiency.

$$N_{max} = \frac{v}{k\dot{A}}ln\left(\frac{kQC^{\circ}}{Pi_{tot}E}\right) \quad 5\text{-}17$$

Note that N_{max} is only positive when $kQC^{\circ} > \mathrm{Pi}_{\mathrm{tot}}\mathrm{E}$. This allows for a quick test to see what conditions are worth considering.

Under experimental conditions and theoretically ideal conditions, the best-case operating cost for the INCO SO_2/Air process is always more cost effective than electrolysis. However, Electrolysis becomes even more efficient the greater the initial cyanide concentration becomes. While this analysis assumes $C^{\circ} = 0.25\ \mathrm{kg/m^3}$, INCO reported concentrations between 0.1 and $0.8\ \mathrm{kg/m^3}$, meaning there are possible operating conditions for which early-stage electrolysis is cost effective in terms of operating costs.

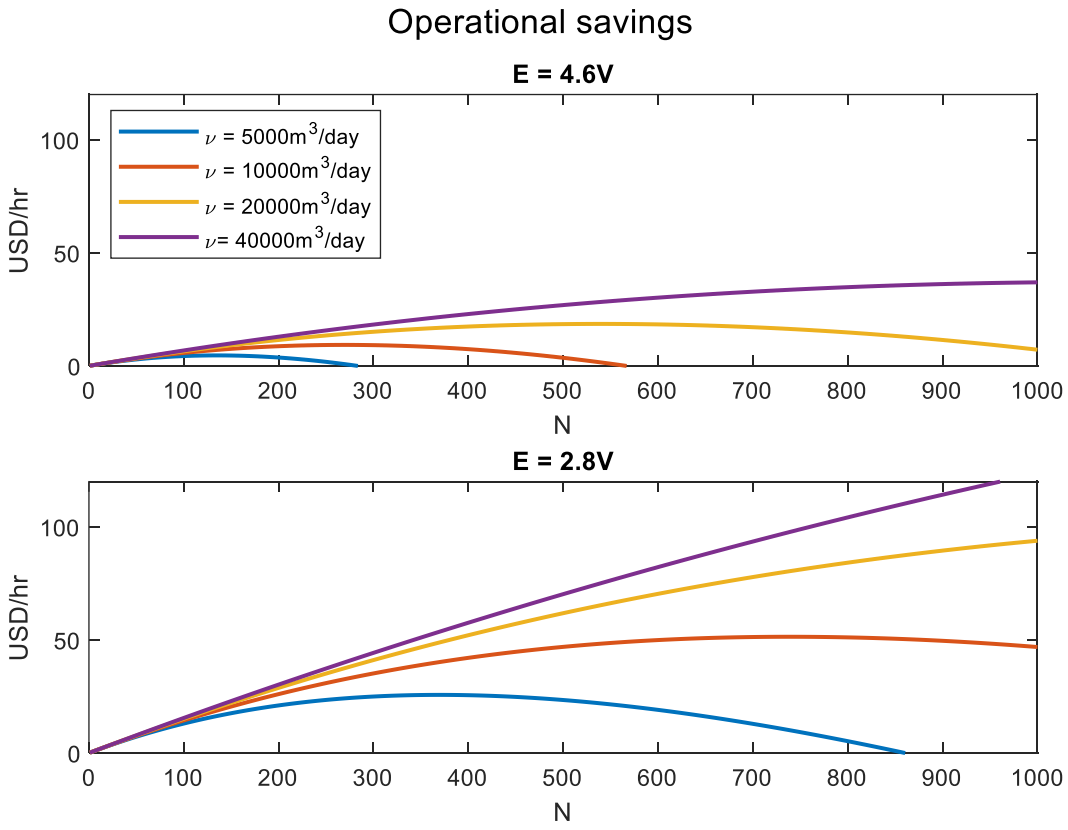

Figure 5-2: savings per hour of electrolysis—SO_2/Air in series over just SO_2/Air assuming an initial cyanide concentration of 250 ppm and an SO_2/Air process operating cost of 2.86 USD/kg

At the median operating cost, electrolysis in the early stages is always cost effective. Figure 5-2 shows the operating cost savings of using electrolysis in series with SO_2/Air for N stages of initial electrolysis. For very large flowrates under theoretically optimal voltages, N_{max} exceeds the validity of Equation 5-7.

5.3.2 Maximizing IRR

The internal rate of return is the rate of return at which the net present value is 0 dollars. It is the maximum capital cost that can be assumed in order to break even on a project. Maximizing the IRR is therefor ideal. Over an infinite timespan, the IRR could be taken as the ratio between the $Capital\ Cost$ and the $Cost\ Savings$. Realistically, however, the annuity factor in Equation 5-14 decays exponentially from 0 to a value of R^{-1}. The lifetime of a project is unlikely to approach that limit of R^{-1} unless R is very large, or the project lifetime is unrealistically long.

If $Capital\ Cost$ was fixed or independent of N, Equation 5-17 could be taken as the most cost-effective flow cell size. However, if the growth in capital cost as flow cell size grows is significant, as is true in most cases, Equation 5-17 serves as an upper bound for a financially feasible reactor size.

The maximum IRR occurs at the minimum payback period. The goal, then, is to determine the number of cells N that minimizes the right side of Equation 5-18.

$$\left(\frac{1-(1+R)^{-T}}{R}\right) = \frac{\alpha(N)^{\beta}}{vC^{\circ}Q\left(1-e^{-\frac{k\dot{A}N}{v}}\right) - Pi\dot{A}NE} \qquad 5\text{-}18$$

Figure 5-3 shows the plots of the payback period for a flow cell with a 2 cm spacing. On inspection, the system is not financially feasible, showing a payback period on the order of hundreds of years. Table 5-2 also demonstrate that IRR is never positive for an a typical mine life of 20 years. With a 6.5 cm spacing, the performance was even worse, with payback periods exceeding 600 years.

Table 5-2: Optimal number of electrolytic reactors with 2 cm electrode spacing and corresponding payback period and IRR as a function of daily flow rate of 250 ppm cyanide effluent.

$v\ m^3/day$	*Optimal* N	*Payback period*	*IRR for 20 year project*
5000	16	259 years	-17.4%
10000	32	254 years	-17.3%
20000	64	249 years	-17.2%
40000	127	244 years	-17.1%

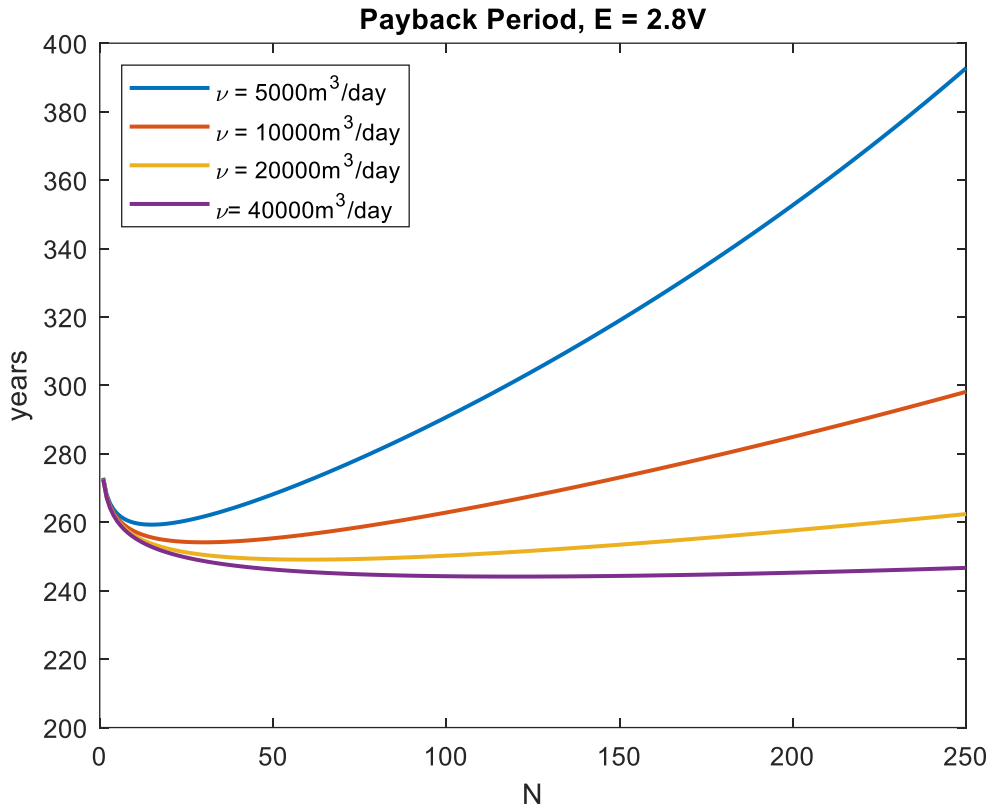

Figure 5-3: payback period of electrolysis—SO_2/air in series over just SO_2/air assuming an initial cyanide concentration of 250 ppm and an SO_2/air operating cost of 2.86 USD/kg

6 FUTURE WORK

Future work for electrolytic cyanide destruction should proceed with improvements to the arrangement of the electrolytic cells during experiments as well testing more novel cell designs rather than simple parallel plate design employed in this study. Also, alternative materials of construction should be studied.

6.1 ALTERNATIVE EXPERIMENTAL CELL ARRANGEMENT

Section 5 shows evidence of mass transport limited cyanide destruction; however, the model is only a rough fit. Ideally there would be more data points to allow for better model exploration. One of the inhibitions of this study was balancing data collection with safety. Ideally each cell solution would be created from the same stock, however mixing and storing large amounts of cyanide solution is unsafe. To that end, small batches of 2.4 L cyanide solution were created, enough for six cells and left over for batch solution analysis. This eliminated the need for storage of large amounts of cyanide and minimized the time technicians spent interacting with the cyanide. This allowed for three cells containing copper and three cells copper free to be tested in tandem for the same amount of time. Cells that experienced the same time of current application were therefore made from identical electrolyte solution. Since all runs of the same time were made from the same electrolyte, any variance in the preparation of the electrolyte carried over to every data point in that time window.

To address both these concerns, an alternative experimental design is proposed.

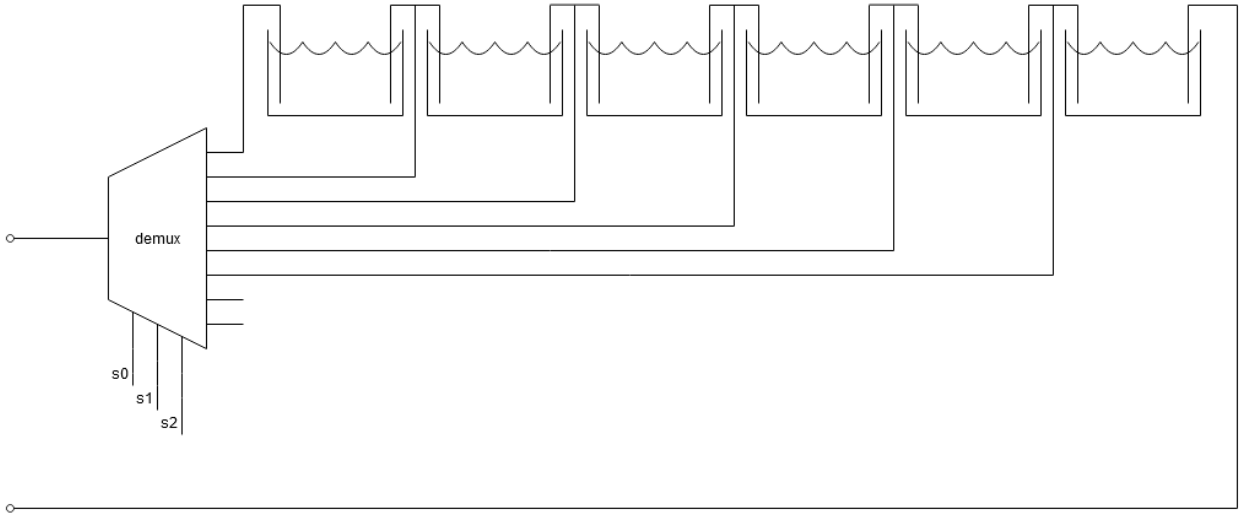

Figure 6-1: alternative circuit design for the experiments described in Section 5.

Using an analog demultiplexer and a timer, the cells can be arranged in series. The demultiplexer output begins as A0, and moves to A1, A2, etc. at regular intervals, causing the current to skip over the earlier cells. Using a galvanostat as a power source, each cell will there for experience the same current without any risk of batch defects impacting the experiment quality. This setup would allow for 7 data points per experiment: one for 0 hours of current application, and 6 for any set of predetermined time windows, though using a 3-bit deMUX as shown in would allow for up to 9 data points. Variations due to batch preparation differences would then also be spread across multiple time windows, eliminating them as an explanation for the differences between observation and the model derived in Section 4

6.2 ALTERNATIVE CELL DESIGN

Section 5.3 showed that electrolysis in series with the INCO SO_2/Air process is cost effective but only over unrealistically long time frames. Some approaches are worth considering to bring the payback period down to a reasonable value. The major hindrance in financial feasibility is the capital cost as the flow cell requires a very large area to be effective. One quick

way to judge the effectiveness of a cell design is the area to volume ratio. In Equation 5-2 this ratio is expressed as $1/w$, where w is the spacing between electrodes. For a given flow-cell volume, a larger $1/w$ ratio will perform better.

6.2.1 Cylindrical cells

One alternative design is to use concentric cylindrical electrodes rather than parallel plates. The electrode of interest (anode) is the outer cylinder, with the counter electrode (cathode) as the inner cylinder. This type of design is employed by Electrometal in their EMEW cell.

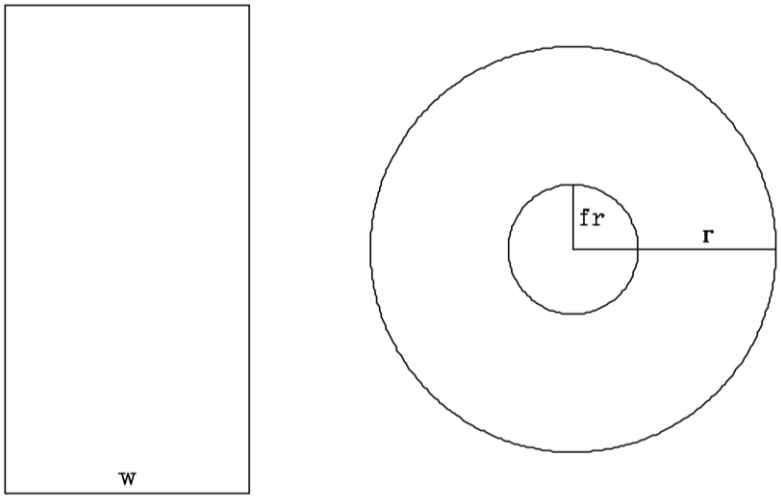

Figure 6-2: cross sectional area of parallel plate cell (left) and a cylindrical cell (right).

The electrode area to volume ratio can be examined using the cross section of the flow cell as the ratio between the arc length of the electrode cross section and the total area. Taking the radius of the anode as r and the radius of the cathode as fr where f is the ratio between anode and cathode radii:

Anode arc length	*Flow surface area*	$\frac{A}{V}$
$2\pi r$	$\pi r(1-f^2)$	$\frac{2}{r}\left(\frac{1}{1-f^2}\right)$

Taking the same electrode spacing, w, as $r(1-f)$:

$$\frac{A}{V}=\frac{2}{w}\left(\frac{1}{1+f}\right) \qquad 6\text{-}1$$

For $f \in [0,1)$, the area to volume ratio will always be better for the cylindrical flow cell. This would allow for a greater surface area density within the flow cell volume, potentially reducing the capital costs of the flow cell.

6.2.2 Porous cells

Another option is to use a porous anode rather than a parallel design. This design is frequently used in gold electrowinning, which features poor current efficiency (frequently <10%) [3] [2], using steel mesh/wool cathodes to maximize cathode area. However, this design would fall outside the scope of the data and models developed in Section 5 and would require separate experiments to determine the necessary rate constants for cell design. It also makes the design difficult to study and predict beyond its overall empirical behaviour; the parallel designs above ensure that each point of the electrodes experience similar current densities. That can't be done for porous electrodes.

Porous designs can achieve a A/V ratio on the order of $2.5 \times 10^5/\mathrm{cm}$ in contrast to the parallel plate design above, which considered A/V ratios between $0.25/\mathrm{cm}$ and $0.5/\mathrm{cm}$. This

would massively decrease the plant size required to sufficiently oxidize cyanide is a waste stream.

6.3 MATERIALS OF CONSTRUCTION

Alternative materials of construction should be explored in future studies. 304 stainless steel was selected as a relatively cheap material of construction for the electrodes, due to its general corrosion resistance under alkaline conditions. However, it did show signs of susceptibility to corrosion, particularly at high current densities. Hence, the use of other more corrosion resistant stainless steels, such as 316, might be explored in future studies.

7 BIBLIOGRAPHY

[1] B. Yarar, "Long term persistence of cyanide species in mine waste environments," in *Tailings and Mine Waste 2002: Proceedings of the 9th International Conference*, 2002.

[2] N. Brandon, M. Mahmood, P. Page and C. Roberts, "The Direct Electrowinning of Gold from Dilute Cyanide Leach Liquors," *Hydrometallurgy,* 1987.

[3] J. O. Marsden and C. I. House, The Chemistry of Gold Extraction, Society for Mining, Metallurgy, and Exploration, Inc., 2006.

[4] R. Eisler and S. N. Wiemeyer, "Cyanide Hazards to Plants and Animals from," *Reviews of Environmental Contamination and Toxicology,* 2004.

[5] "SCHEDULE 4: Authorized Limits of Deleterious Substances," 15 05 2021. [Online]. Available: https://laws-lois.justice.gc.ca/eng/regulations/SOR-2002-222/section-sched685007.html. [Accessed 17 05 2021].

[6] P. Breuer, C. Sutcliffe and R. Meakin, "Comparison of industrial cyanide destruction processes," in *25th International Mineral Processing Congress - IMPC2010*, Brisbane, Qld, Australia, 2010.

[7] T. I. Mudder, M. M. Botz and A. Smith, Chemistry and Treatment, London: Mining Journal Books Ltd, 2006.

[8] S. C. Cheng, M. Gatrell, T. Guena and B. MacDougal, "The electrochemical oxidation of alkaline copper cyanide solutions," *Electrochimica Acta,* vol. 47, 2002.

[9] A. Katagiri, S. Yoshimura and S. Yoshizawa, "Formation Constant of the Tetracyanocuprate(I1) Ion and the Mechanism of Its Decomposition," *Inorganic Chemistry,* 1981.

[10] P. Beuer, C. Jeffery and R. Meakin, "Fundamental investigations of the So2/Air, peroxide and caro's acid," in *CSIRO Symposium*, 2011.

[11] B. Wels and D. C. Johnson, "Electrocatalysis of Anodic Oxygen Transfer Reactions: Oxidation of Cyanide at Electrodeposited Copper Oxide Electrodes in Alkaline Media," *Journal of the Electrochemical Society,* 1990.

[12] F. Hine, M. Yasuda, T. Iida and Y. Ogata, "On the oxidation of cyanide solutions with lead dioxide coated anode," *Electrochemica Acta,* 1986.

[13] G. H. Kelsall, S. Savage and D. Brandt, "Cyanide Oxidation at Nickel Anodes II. Voltammetry and Coulometry of Ni/CN-H20 Systems," *Journal of The Electrochemical Society,* 1991.

[14] C. Comninellis, "Electrocatalysis in the electrochemical conversion/combustion of organics pollutants for waste water treatment," *Electrochemical Society,* 1994.

[15] J.-Y. Hwang, Y.-Y. Wang and C.-C. Wan, "Electrolytic oxidation of cuprocyanide electroplating waste waters under different pH conditions," *JOURNAL OF APPLIED ELECTROCHEMISTRY,* 1987.

[16] M. R. Lanza and R. Bertazzoli, "Cyanide Oxidation from Wastewater in a Flow Electrochemical Reactor," *Industrial and Engineering Chemistry Research,* 2002.

[17] Z. Wei, T. Zhao, X. Zhu and P. Tan, "MnO2-x nanosheets on stainless steel felt as a carbon- and binder-free cathode for non-aqueous lithium-oxygen batteries," *Journal of Power Sources,* 2015.

[18] J. Gonzalas, "Zinc electrowinning: anode conditioning and current distribution studies," in *Electrometallurgy 2001: Proceedings of the 31 st Annual Hydrometallurgy Meeting as held at the 40 th*, 2001.

[19] G. M. Jacob and I. Zhitomirsky, "Microstructure and properties of manganese dioxide films prepared by," *Applied Surface Science,* 2008.

[20] J. A. Gonzolez-Dominguez and R. W. Lew, "Evaluating Additives and Impurities in Zinc Electrowinning," *JOM,* 1995.

[21] B. Beverskog and I. Puigdomenech, "Pourbaix Diagrams for the Ternary System of Iron-Chromium-Nickel," *Corrosion,* 1999.

[22] M. Drogowska, H. Menard and L. Brossard, "Electrodoxidation of stainless steel AISI 304 in carbonate aqueous solution at pH 8," *Journal of Applied Electrochemistry.*

[23] P. L. Breuer, C. A. Sutcliffe and R. L. Meakin, "Cyanide measurement by silver nitrate titration: Comparison of rhodanine and potentiometric end-points," *Hydrometallurgy,* 2010.

[24] P. Wei, M. Bieringer, L. M. Cranswick and A. Petric, "In situ high-temperature X-ray and neutron diffraction of Cu–Mn oxide phases," *Journal of Materials Science,* 2009.

[25] C. Stinn and A. Allanore, "Estimating the Capital Costs of Electrowinning Processes," *The Electrochemical Society,* 2020.

[26] "CRC Handbook of Chemistry and Physics, 91th edition," 2004.

[27] M. E. Lyons, R. L. Doyle, D. Fernandez, I. J. Godwin, M. P. Browne and A. Rovetta, "The mechanism and kinetics of electrochemical water oxidation at oxidized metal and metal oxide electrodes. Part 2. The surfaquo group mechanism: A mini review," *Electrochemistry Communications,* 2013.

[28] A. Valiūnienė, G. Baltrūnas, V. Keršulytė, Ž. Margarian and G. Valinčius, "The degradation of cyanide by anodic electrooxidation using different anode materials," *Process Safety and Environmental Protection,* 2013.

[29] A. Adachi, S. Nojima, Y. Hagiwaras, M. Hamamoto and T. Kobayashi, "Studies on the oxidative decomposition of cyanide ion by potassium permanganate," *Environmental Technology,* 2008.

APPENDIX

1 CHEMICALS, MATERIALS, EQUIPMENT, AND INSTRUMENTATION

1.1 LIST OF CHEMICALS

Chemicals	Grade	Manufacturer
NaOH	ACS	Fisher
$HNaCO_3$	ACS	Sigma-Aldrich
Na_2CO_3	ACS	Sigma-Aldrich
NaCN	ACS	Anachemia
$CuSO_4 \cdot 5H_2O$	USP	Fisher
H_2SO_4	ACS	Fisher
$KMnO_4$	ACS	Sigma-Aldrich
KCl	ACS	Sigma-Aldrich
$AgNO_3$	ACS	Sigma-Aldrich
pH4 buffer		Fisher
pH7 buffer		Fisher
pH10 buffer		Fisher

1.2 LIST OF MATERIALS

Material	Grade	Manufacturer
304 stainless steel	N.A.	McMaster-Carr
PVC	N.A.	McMaster-Carr

2 FREQUENCY RESPONSE ANALYSIS

Frequency response analysis was used to explore the kinetics of cyanide oxidation. Using the result from Section 4.1.2 as a starting point, frequency response was done at a range of potentials between 1000 mV and 1500 mV vs Ag/AgCl/KCl(sat). The resulting impedance was used to generate a Nyquist plot. The expectation was that if the system demonstrated Warburg impedance at the applied potential, it would indicate that cyanide was being oxidized at its mass transport limiting rate.

2.1.1 Methodology

The cells were constructed as described in Section 3.1.1. The voltage frequency was applied on top of a range of voltages between 1 V and 1.5 V vs Ag/AgCl/KCl(sat) using an AUTOLAB PSTAT100. Fifty frequencies were applied between 1 Hz and 10 kHz. The experiment was conducted with and without presence of copper at 10 mg/L (introduced as 24 mg/L of $CuSO_4$).

2.1.2 Results

Notably, steel electrodes in presence of copper had the lowest overall impedance. The MnO_2 layer showed a much larger capacitance, as expected. The presence of copper significantly reduced the capacitance and increased the real impedance, suggesting some interaction between the copper ions and the MnO_2 layer.

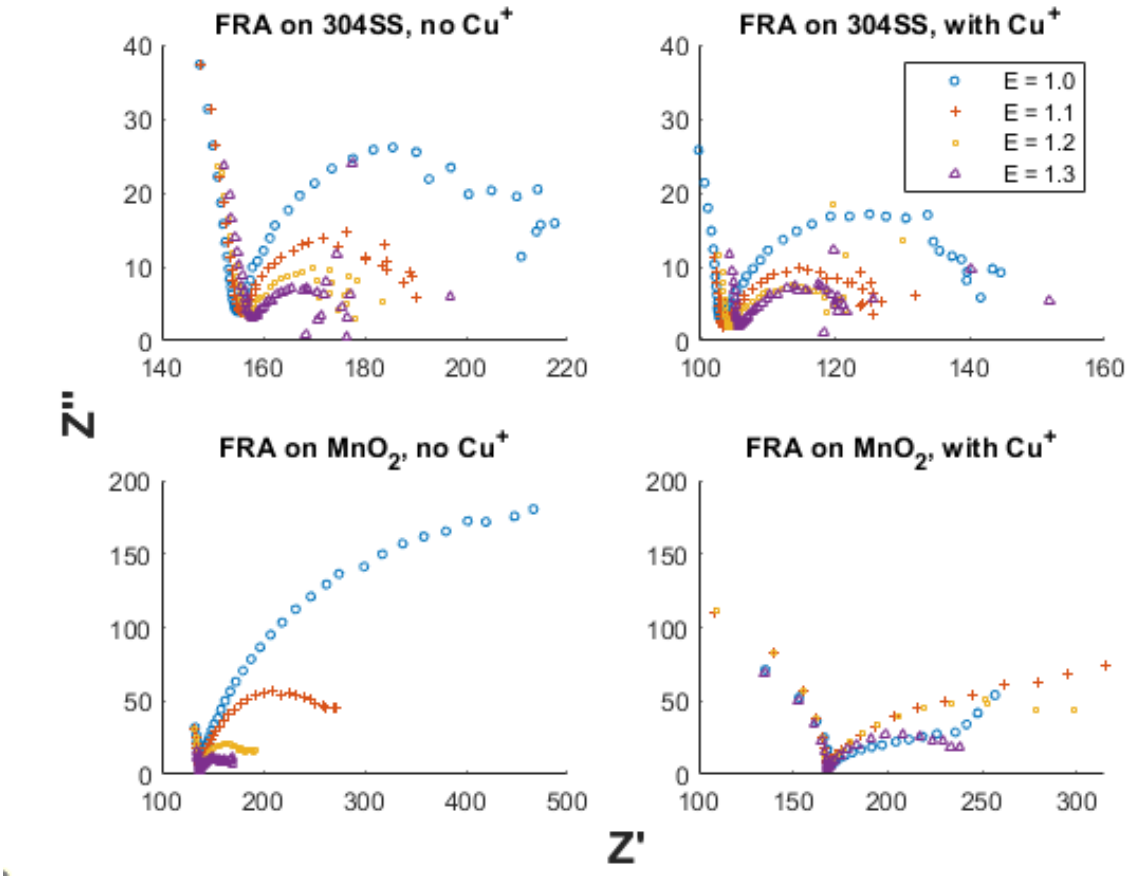

Figure 2-1: FRA on bare steel (top) and MnO_2 (bottom) with and without copper (left and right, respectively).

At 1.2 V and 1.3 V vs Ag/AgCl/KCl(sat), the Nyquist plots for copper-less MnO_2 electrodes were suggestive of a Warburg element in the circuit. Similar, MnO_2 in presence of copper shows a clear Warburg element at 1 V. However, these results are inconsistent, and the formation of oxygen on the electrode surface impedes more precise analysis.

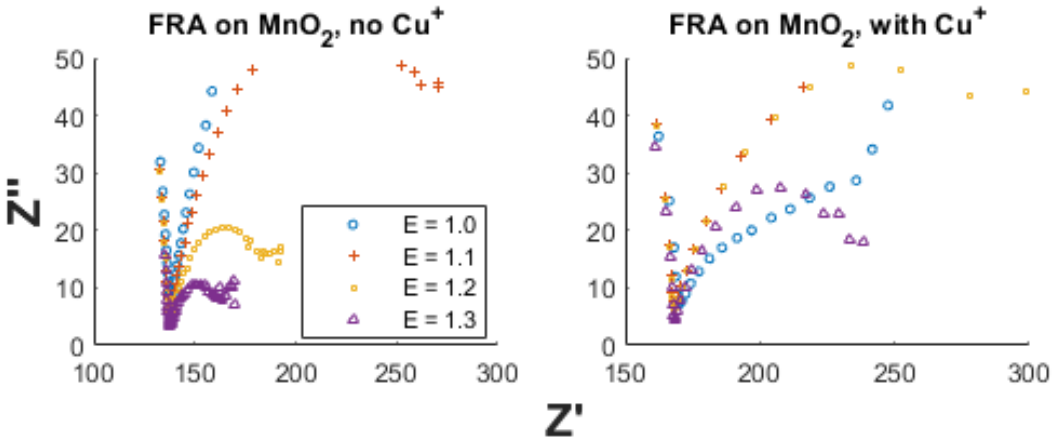

Figure 2-2: FRA on MnO_2 between 0 and 50 ohms of imaginary impedance.

3 ICP-MS Analysis Results

The following graphs show the evolution of residual ion concentration for chrome, nickel, iron and manganese ions as measured by ICP-MS analysis performed by the Perdue Central Analytical Facility after galvanostatic electrolysis as described in Section 4.2. In several cases, the residual concentration was below the detection limit, so no value is reported. Solution samples prior to electrolysis were also analyzed and universally showed no elements of interest.

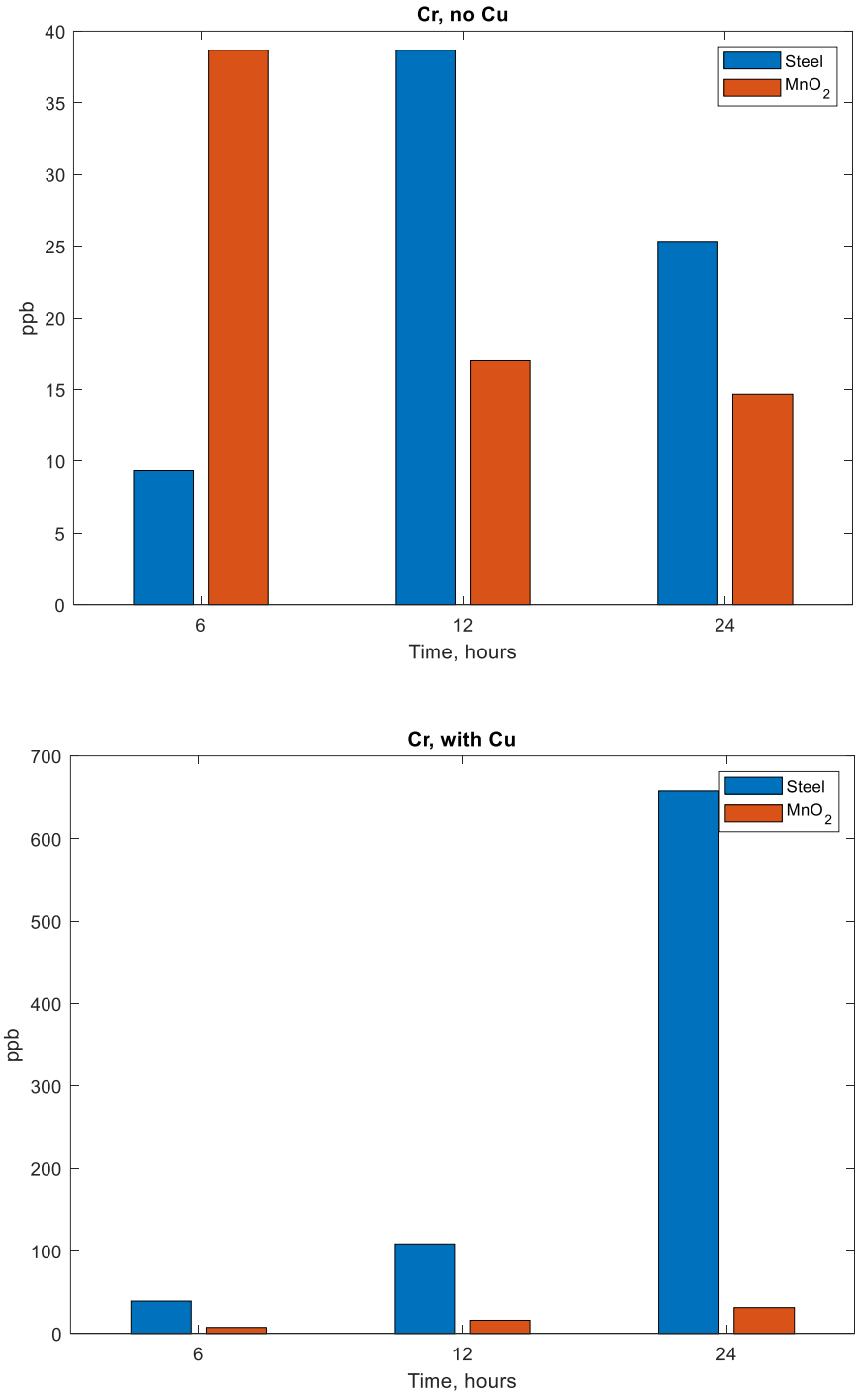

Figure 3-1: Residual chrome concentrations in ppb after 6, 12, and 24 hours of electrolysis at 2 mA/cm^2 without copper (top) and in presence of copper (bottom).

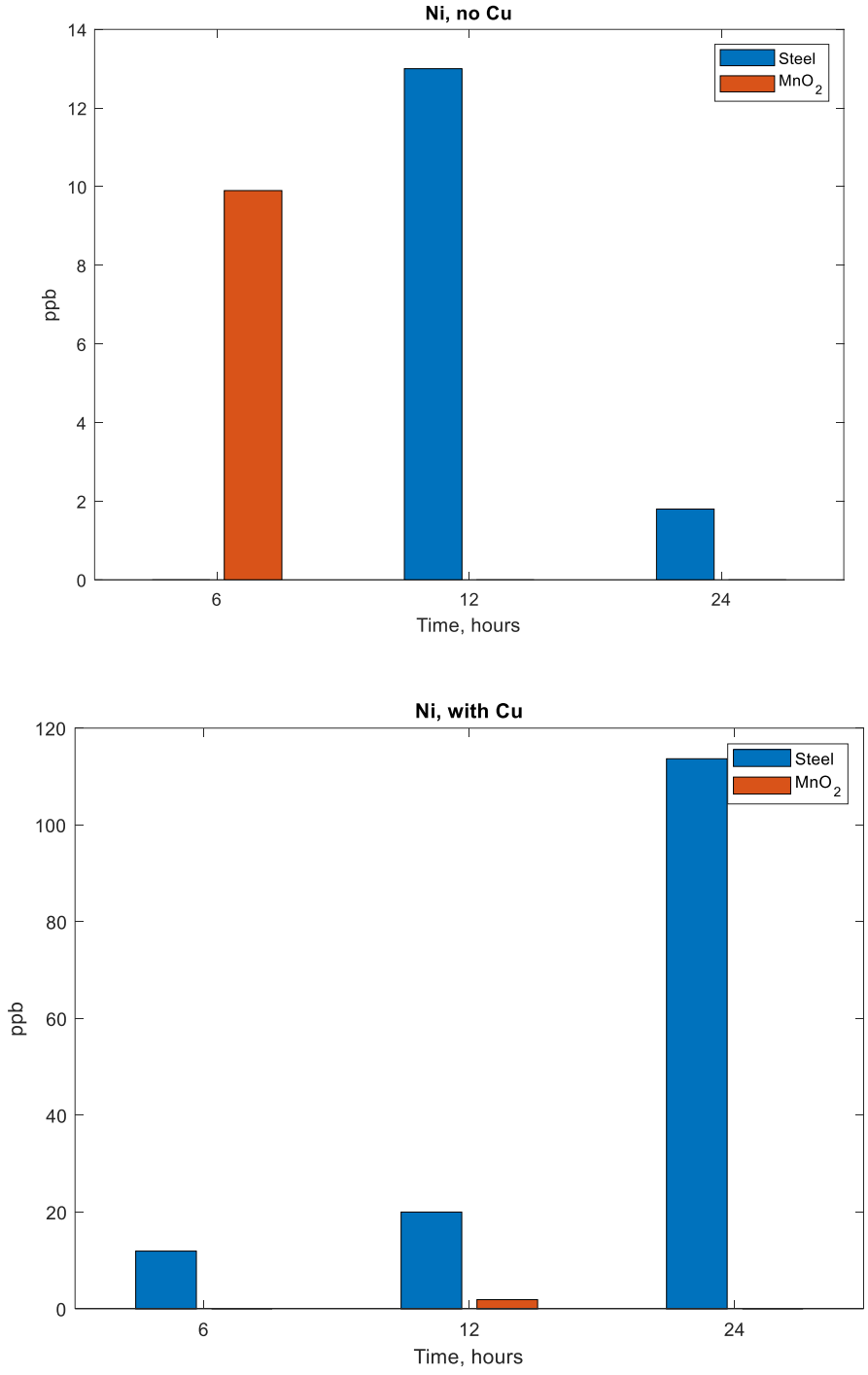

Figure 3-2: Residual nickel concentrations in ppb after 6, 12, and 24 hours of electrolysis at 2 mA/cm² without copper (top) and in presence of copper (bottom).

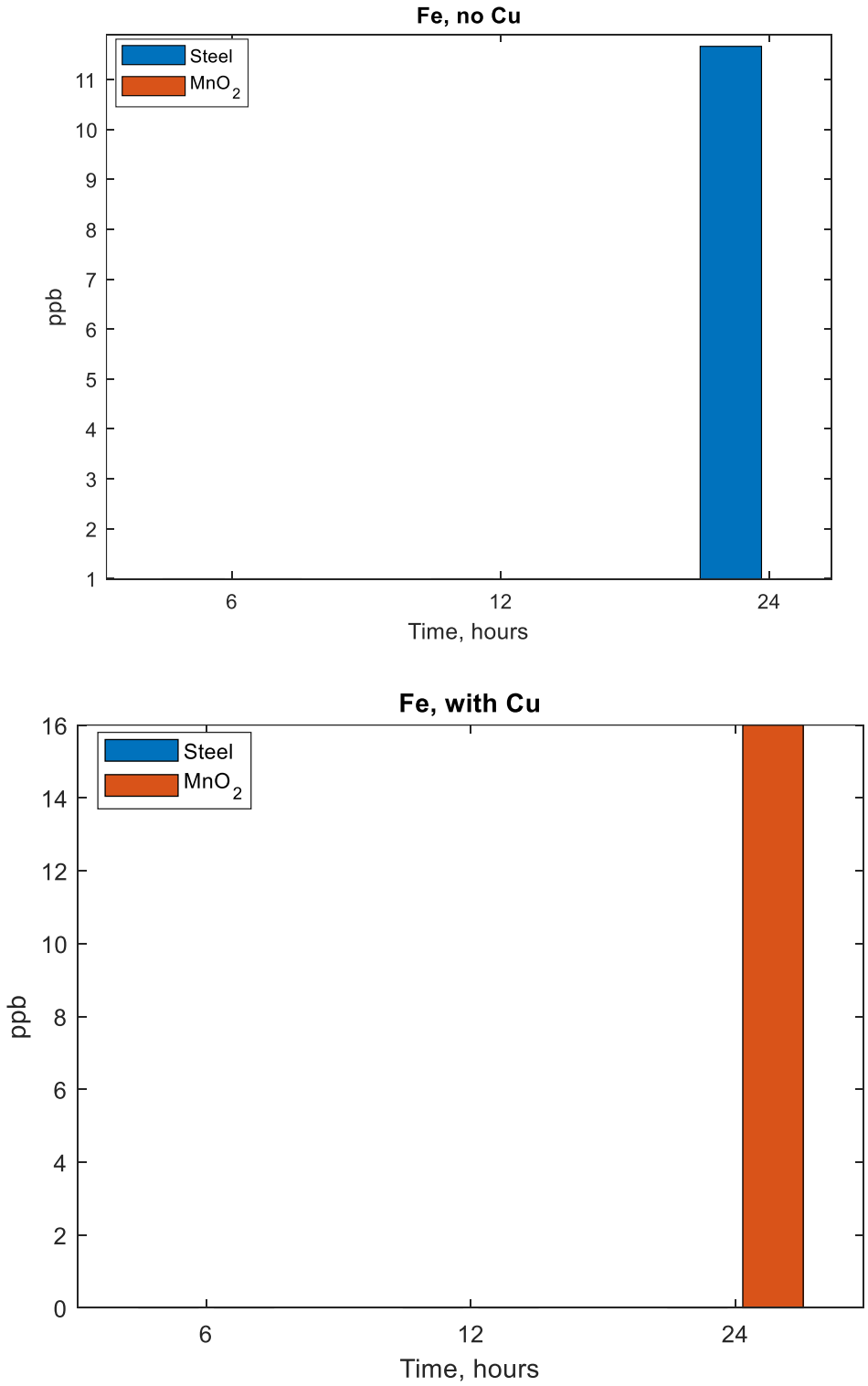

Figure 3-3: Residual iron concentrations in ppb after 6, 12, and 24 hours of electrolysis at 2 mA/cm^2 without copper (top) and in presence of copper (bottom).

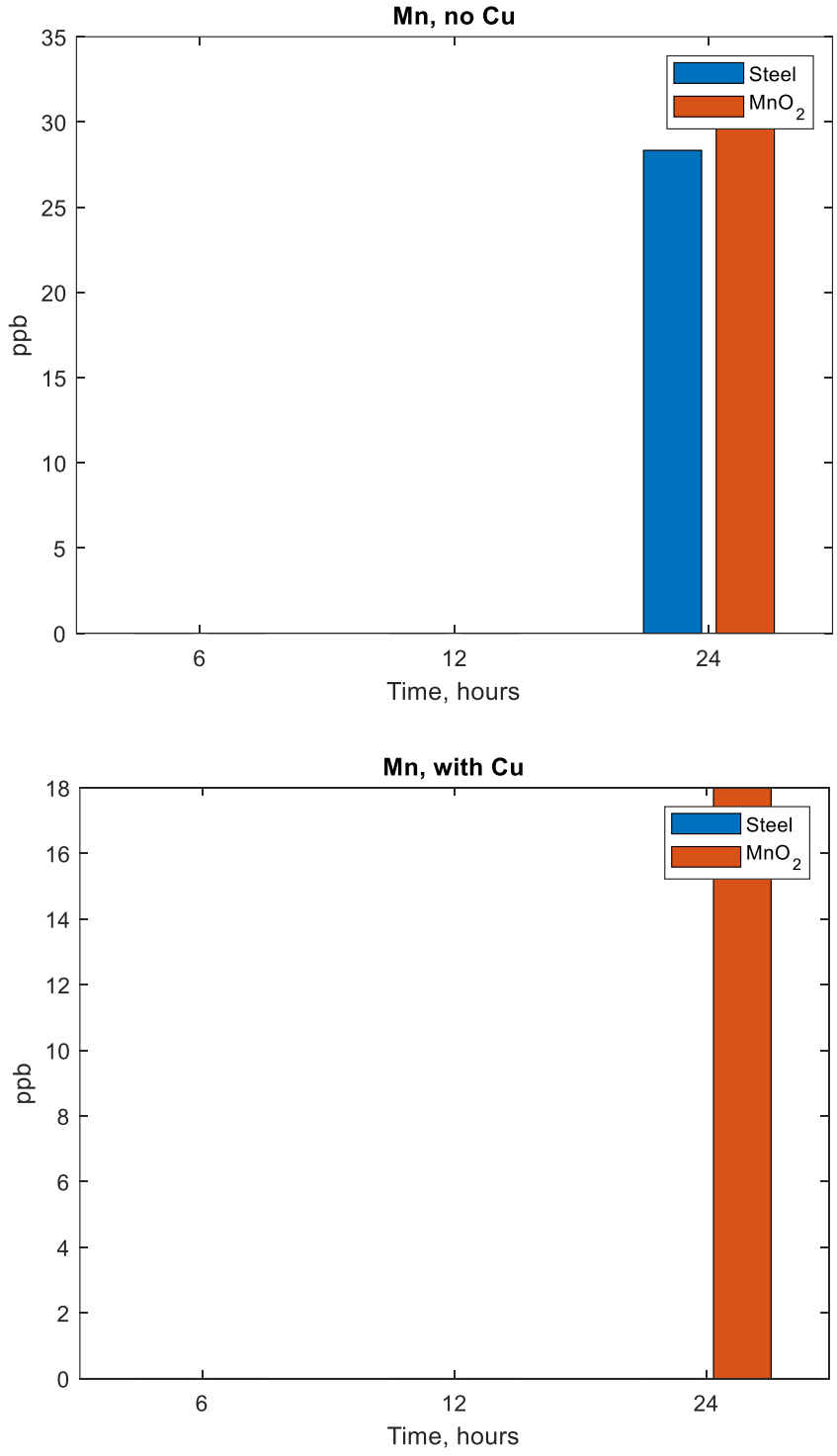

Figure 3-4: Residual manganese concentrations in ppb after 6, 12, and 24 hours of electrolysis at 2 mA/cm^2 without copper (top) and in presence of copper (bottom).